Cycling phosphorus on the Archean Earth: Part II. Phosphorus limitation on primary production in Archean ecosystems

Jihua Hao, Andrew H. Knoll, Fang Huang, Juergen Schieber, Robert M. Hazen, Isabelle Daniel

Feb-24-2020

Cycling Phosphorus on the Archean Earth: Part II. Phosphorus Limitation on Primary Production in Archean Ecosystems

Authors: Jihua Hao[1,2*], Andrew H. Knoll[3], Fang Huang[4,5], Juergen Schieber[6], Robert M. Hazen[7], Isabelle Daniel[1]

*Corresponding author: haojihua@gmail.com

[1]Univ Lyon, Université Lyon 1, Ens de Lyon, CNRS, UMR 5276 LGL-TPE, F-69622, Villeurbanne, France

[2]Department of Marine and Coastal Sciences, Rutgers University, New Brunswick NJ, 08901, USA

[3]Department of Organismic and Evolutionary Biology, Harvard University, Cambridge MA 02138, USA

[4]Tetherless World Constellation, Rensselaer Polytechnic Institute, Troy NY, 12180, USA

[5]CSIRO Mineral Resources, Kensington, WA 6151, Australia

[6]Department of Earth and Atmospheric Sciences, Indiana University, Bloomington, IN, 47405, USA

[7]Geophysical Laboratory, Carnegie Institution for Science, Washington DC, 20015, USA

Abstract:

Several lines of evidence point to low rates of net primary production (NPP) in Archean oceans. However, whether Archean NPP was limited by electron donors or nutrients, particularly phosphorus (P), and how these factors might have changed over a billion years of recorded Archean history, remains contentious. One major challenge is to understand quantitatively the biogeochemical cycling of P on the early Earth. In Part I of this series (Hao et al., 2020), we estimated the weathering flux of P to the oceans as a function of temporally increasing continental emergence and elevation through Archean time. In Part II, we conduct thermodynamic and kinetic simulations to understand key processes of P cycling within the Archean ocean, including seafloor weathering, recycling of organic P, the solubility and precipitation of secondary phosphate minerals, and the burial diagenesis of P precipitates. Our calculations suggest low solubilities of apatite minerals in Archean seawater, primarily due to nearly neutral pH and high levels of Ca. This low solubility, in turn, implies a negligible contribution of apatite dissolution to P bioavailability in Archean seawater.

We also simulate the solubility limits of common secondary P-bearing minerals, showing that vivianite would have been the least soluble P mineral in ferruginous Archean seawater (0.1 to 0.3 μM), even at moderate supersaturation states (Ω = 100 or 1000). If vivianite precipitation was kinetically favorable by microbial activities and mineral adsorption, the sinking flux of P as vivianite in Archean seawater could have reached the modern sinking flux, implying that vivianite precipitation was a potentially major sink for P in Archean oceans. During burial diagenesis, however, vivianite in porewater would have become less stable than Ca-phosphates of lower solubility. At elevated temperatures (>100 °C) associated with burial diagenesis and low-grade metamorphism, vivianite is predicted to react irreversibly with calcite to form apatite.

Optimistic assumptions about the recycling efficiency of P on the Archean Earth lead us to estimate that by the end of the eon the total flux of P (continental weathering + recycling) could have supported NPP at levels up to 7 % of the modern. The total flux of P would have been much lower on the early and middle Archean Earth, whereas fluxes of electron donors could have been higher, suggesting very low productivity and P-limitation of marine ecosystems during much of the eon. Comparing our estimates of NPP as limited by P supply with the estimate by Ward et al. (2019), in which NPP was limited by electron donors and metabolic efficiency, there could have been a transition between P-limited productivity in the early to middle Archean to electron donor-limitation closer to the eon's end (assuming no oxygenic photosynthesis). Once oxygenic photosynthesis reached ecological significance, probably near the end of the Archean, our estimated flux of P would allow rapid oxidation of atmosphere.

(466/500 words)

Keywords: vivianite; phosphorus recycling; burial diagenesis; apatite nodules; primary production; oxygenation of atmosphere. (6/6 keywords)

1. Introduction

How productive were Archean oceans? All recent estimates of Archean primary production are low (Bjerrum & Canfield, 2002; Canfield et al., 2006; Kharecha et al., 2005; Laakso & Schrag, 2018; Ward et al., 2019), but there is no consensus just how low they were, nor on the principal factors that limited photosynthesis in early ecosystems. Some commentators posit that prior to the evolution of oxygenic (cyanobacterial) photosynthesis, the global availability of electron donors would have constrained rates of primary production to low levels. For example, Canfield et al. (2006) estimated the abundances of non-water electron donors in Archean oceans, concluding that the most abundant species, Fe^{2+}, would have supported primary production at levels up to 10% of the modern. In contrast, Ward et al. (2019) argued that H_2 and, to a lesser extent, Fe^{2+} together fueled early photoautotrophy at rates well below one percent of modern levels. And recently, Tosca et al. (2019) concluded that photoautotrophy of ferrous iron could have made only a negligible contribution to productivity in early oceans. In contrast, some analyses point to nutrient limitation in early oceans, specifically suggesting that relatively low phosphate availability could have limited primary production, even at low ferrous iron availability (Kipp and Stüeken, 2017); others propose that P was relatively bioavailable, especially as phosphite (Herschy et al., 2018).

Of particular interest is the role that oxygenic photoautotrophs may have played prior to the Great Oxygenation Event (GOE) ca. 2.4 billion years ago. It has been proposed that the GOE simply reflects the evolution of oxygenic photosynthesis (e.g., Fischer et al., 2016; Kopp et al., 2005), but this view is challenged by both an increasing inventory of geochemical evidence for earlier “whiffs of oxygen” (Anbar et al., 2007; Kaufman et al., 2007) and molecular clocks that call for the evolution of coupled photosystems capable of extracting electrons from water as early as 3.2 Ga (Cardona et al., 2019). Of course, if P availability strictly limited rates of primary production on the Archean Earth, oxygen

production may well have been too low to titrate available reductants, even if oxygenic photosynthesis was relatively prominent.

To explore these issues further, we employ kinetic and thermodynamic modeling to estimate P availability in the global scale of seawater through a billion years of recorded Archean history.

2. Methods

The bioavailability of P in the sunlit ocean primarily reflects two fluxes: continental weathering and P recycling within the ocean. Considering that Archean seawater was weakly acidic (Halevy and Bachan, 2017; Krissansen-Totton et al., 2018) and reducing, seafloor weathering might also have been a significant source of P on the early Earth. In Part I of this series (Hao et al., 2020), we simulated the input of P to the Archean oceans from continental weathering and erosion, concluding that P fluxes from land were extremely low as the Archean Eon began but increased to values similar to the modern by the time the eon ended. In this study, we calculate the solubility limits of primary and secondary P-minerals in Archean seawater and porewater environments, simulating seafloor weathering and the precipitation of phosphate minerals in and beneath the Archean ocean. We focus in particular on the precipitation of vivianite, as this precipitation has been argued to be a major sink for phosphate in ferruginous Proterozoic oceans (Derry, 2015). With these calculations in hand, we assess P recycling in Archean oceans and estimate the total flux of P for net primary production (NPP). Lastly, we consider the fate of P-precipitates during diagenesis and metamorphism, based on both simulations and geological observation.

Our calculations focus on the global-scale evolution of Archean environments. We understand that the Archean Earth was environmentally heterogeneous, with probable local variations in temperature, Fe(II) concentration between seawater and hydrothermal fluids,

redox variation between globally anoxic and locally oxygenated habitats in the late Archean, and variations in the concentration of Fe(II) and S(II) between globally ferruginous seawater and regionally sulfidic seafloor in late Archean oceans. Such heterogeneities are important in considerations of Archean evolution and may influence Archean P cycling, as discussed below. Nonetheless, we argue that our focus on global conditions is most relevant for understanding the P cycle and how it changed through Archean time.

2.1 Archean seawater and porewater chemistry

The emergence of land masses in the middle to late Archean Eon (Hawkesworth et al., 2017), with its consequences for weathering and erosional fluxes, strongly affected marine geochemistry (Bindeman et al., 2018). The evolution of seawater pH and major salts (Ca and Mg) has recently been modeled independently by Halevy and Bachan (2017) and Krissansen-Totton et al. (2018), with similar results. In Part I of this series (Hao et al., 2020), we modified Krissansen-Totton et al.'s (2018) geologic carbon cycle (GCC) model by incorporating continental emergence (Flament et al., 2013; Korenaga et al., 2017) and the weathering kinetics of P, using this modification to simulate the continental flux of P into the oceans (**Table 1**). The GCC model also outputs major component compositions of the atmosphere (including $pCO_{2,g}$) and seawater (including pH, Ca^{2+}, and CO_3^{2-}), and by linking these factors to continental emergence models and solubilities of P-bearing minerals (**Table S2**) we can examine seafloor weathering and the precipitation of P in the Archean oceans (*Sec. 2.2*). In addition, the GCC model allows us to consider the chemistry of porewater, enabling us to explore the post-depositional fate of seafloor P-precipitates (*Sec. 2.5*).

In addition to the above-mentioned species, our simulations require that we input abundance values for other components of seawater and porewaters. A large, recently compiled dataset of fluid inclusions in Archean quartz from different localities supports the

141 view that the concentration of NaCl in Archean seawater was similar to that of the modern
142 (Marty et al., 2018). Accordingly, we assumed that the Cl^- concentration of Archean seawater
143 was the same as today's. F^- concentration is set to be limited by the solubility of fluorite in
144 Archean seawater and porewater, as it is for modern seawater.

145 It has been proposed that Fe^{2+} in Archean seawater was limited by the solubility of
146 amorphous greenalite, experimentally shown to precipitate readily in equilibrium with Fe(II)
147 and silica in anoxic water (Tosca et al., 2016; Tosca et al., 2019). Consistent with these
148 factors, greenalite occurs abundantly in marine sediments, especially in Archean sedimentary
149 successions (Isson and Planavsky, 2018; Johnson et al., 2018). In comparison to greenalite,
150 siderite precipitation is kinetically sluggish under Archean conditions, occurring only when
151 $pCO_{2,g}$ reaches extreme levels, e.g. > 1 bar (Jiang and Tosca, 2019). In the absence of a
152 skeletal silica sink, dissolved silica concentration would presumably have been relatively
153 high, limited by the solubility of amorphous silica (Siever, 1992; Tréguer and De La Rocha,
154 2012). Previous workers have also pointed to green rust as a potentially major precipitate
155 from early seawater (Halevy et al., 2017; Tosca et al., 2019), but its precipitation requires
156 either a flux of $O_{2,g}$ or water pH > 8.0 under anoxic conditions, unlike the anoxic and weakly
157 acidic seawater likely during most of the Archean Eon. Moreover, the precipitation of green
158 rust is sensitive to salinity, and the potential effects of elevated Archean $SiO_{2,aq}$ on green rust
159 precipitation remain unknown (Tosca et al., 2019). Given these considerations, we calculated
160 the Fe^{2+} concentration in Archean seawater based on the equilibrium constant for amorphous
161 greenalite dissolution derived from recent experiments (Tosca et al., 2016) and the
162 assumption that $SiO_{2,aq}$ concentration was equal to the solubility of amorphous silica. Note,
163 however, that siderite could and did form readily by biological reduction of Fe(III) or
164 diagenesis/metamorphism of organic-C in the sediments (Vuillemin et al., 2019), and so

would potentially have been an important mineral product in porewaters beneath Archean oceans (*Sec. 4.3*).

2.2 Thermodynamic models of P-minerals solubilities

We calculated the solubility limits of common primary and secondary phosphate minerals based on equilibrium constants between each mineral and its dominant aqueous species at a given pH in water, e.g. HPO_4^{2-} (pH > 7.2) and $H_2PO_4^-$ (pH < 7.2) as the dominant phosphate species in this study (**Table S1 & S2)**. Calculations were conducted assuming a warm climate (seawater temperature 25°C), supported by recent climate reconstructions (Krissansen-Totton et al., 2018). Small fluctuation of temperature would be expected to result in only limited changes for reaction constants (e.g. Al-Borno & Tomson, 1994). However, large elevation of temperature would significantly affect reaction constants; therefore, for the calculations in diagenetic and metamorphic environments, we varied temperature to investigate the effect of this variable (see below). Equilibrium constants of the dissolution reactions were calculated by SUPCRT92b (Johnson et al., 1992) (**Table S2)**.

In the modern ocean, the sinking of P is, in general, composed of (co-)precipitation of authigenic minerals (**Table S1**), burial as organic-P, or adsorption onto metal-hydroxides and carbonate (Baturin, 2003; Ruttenberg et al., 2014). In iron-rich, low-salinity estuaries along the Baltic Sea, vivianite ($Fe_3(PO_4)_2*8H_2O$) precipitation accounts for as much as 40% of P removal from ambient waters (Lenstra et al., 2018), and Derry (2015) has proposed that this mineral formed an important sink for P in the ferruginous, low-sulfate seawater of mid-Proterozoic oceans. Derry's hypothesis may apply, as well, to the Archean, but this possibility needs to be tested for the distinct and evolving conditions of Archean seawater (pH, Fe, S, and silica). The solubility constant of vivianite is adopted from a previous experimental study (Al-Borno and Tomson, 1994).

190 $$Fe_3(PO_4)_2 \cdot 8H_2O_{,s} \rightarrow 3Fe^{2+} + 2PO_4^{3-} + 8H_2O \quad (1)$$

191 At pH < 7, $PO_4^{3-} + 2H^+ \rightarrow H_2PO_4^-$. As mentioned above, seawater Fe(II) is presumably
192 controlled by the solubility of amorphous greenalite:

193 $$Fe_3Si_2O_5(OH)_{4,am} + 6H^+ \rightarrow 3Fe^{2+} + 2SiO_{2,aq} + 5H_2O \quad (2)$$

194 where, $SiO_{2,aq}$ is set by the solubility of amorphous silica:

195 $$SiO_{2,am} \rightarrow SiO_{2,aq} \quad (3)$$

196 We can obtain the equilibrium constant of the following reaction by combining the reaction
197 constants of reactions (1-3):

198 $$Fe_3(PO_4)_2 \cdot 8H_2O_{,s} + 2SiO_{2,am} \rightarrow Fe_3Si_2O_5(OH)_{4,am} + 2H_2PO_4^- + 2H^+ + 3H_2O \quad (4)$$

199 In similar fashion, we compiled the reported equilibrium constants of the dissolution
200 reactions of other common secondary P-minerals and calculated their solubility limits in the
201 Archean seawater and porewater (**Table S2**).

202

203 *2.3 Crystallization and precipitation kinetics of vivianite*

204 We employed the crystal growth kinetics of vivianite reported previously (Madsen &
205 Hansen, 2014; Madsen, 2019). Vivianite crystals have shown to follow spiral growth
206 mechanism at low supersaturation states (Madsen & Hansen, 2014) with the rate expression:

207 $$Rs = b(c_{Fe} - c_{Fe,eq})\ln\Omega \quad (5)$$

208 b (nm/s/M) is rate constant, Ω is the saturation state of vivianite defined by the ratio of
209 quotient (Q) and equilibrium constant (K) of the precipitation reaction. Considering that the
210 Archean seawater had high concentrations of Fe^{2+} and vivianite could reach moderate to high
211 supersaturation states (as discussed below), we assume that $c_{Fe} - c_{Fe,eq} \cong c_{Fe}$. The value of b
212 was found to increase with increasing concentrations of Ca^{2+}; due to the limited Ca^{2+} range
213 considered in the literature, we used 3.19 (at 6.11 mM Ca^{2+} in Madsen, 2014) as a
214 conservative value for Archean seawater.

Following the methods proposed by Derry (2015), we simulated the precipitation rate and deposition flux of vivianite as a function of this mineral's saturation state. Simply put, the rate law for vivianite precipitation is

$$R_p = k_{eff}\left[\left(\frac{Q}{K}\right) - 1\right]^n \quad (4)$$

R_p: precipitation rate of vivianite, mole/(m^3*s); k_{eff}: $2.6 \pm 0.3 \times 10^{-15}$ mol/(m^3*s); n: 1.3 ± 0.3. The precipitation flux of vivianite is calculated by integrating the rate over the likely depth of Archean Fe(II)-rich seawater, similar to Derry (2015).

2.4 Recycling of phosphorus in Archean seas

Considering that seafloor weathering (Sec. *3.1 & 4.1*) and extraterrestrial impacts (**Table 1**) provide only small amounts of phosphorus, we assume that the total P for Archean NPP is predominantly composed of P from continental weathering and recycling within the ocean, i.e.,

$$\text{NPP(P)} = \text{Recycling-P} + \text{Weathering-P} \quad (5)$$

Assuming $R_{recycling}$ = recycling efficiency of biological P,

$$\text{Recycling-P} = R_{recycling} * \text{NPP(P)} \quad (6)$$

Therefore,

$$\text{NPP(P)} = R_{recycling} * \text{NPP(P)} + \text{Weathering-P} \quad (7)$$

And,

$$\text{NPP(P)} = \text{Weathering-P}/(1 - R_{recycling}) \quad (8)$$

According to **Table 1**, $R_{recycling}$ = 0.998 in the modern ocean, but due to a limited supply of oxidants and possible precipitation of P as vivianite in the Archean ocean, the recycling of P would have been less efficient. As discussed in detail in *Section 4.4*, we choose $0.01 < R_{recycling} < 0.78$ in the Archean ocean and, based on that value, we calculate the maximum amount of recycled P available for Archean primary producers, as reported in **Table 1**.

240

241 *2.5 Diagenetic and metamorphic transformation of vivianite: modeling*

242 In this study, we simulated the stability and solubility of various phosphate minerals
243 and other diagenetic minerals in porewater environments (**Fig. S1-2**; 25 °C), thereby
244 mimicking the early diagenesis of P in the Archean marine sediment.

245 In addition, we simulated the reaction of vivianite + calcite (+ fluorite as a source of
246 F^-) to form apatite + siderite (+ release of water) at elevated temperatures, mimicking the fate
247 of vivianite during burial diagenesis and metamorphism. The equilibrium constants of the
248 reaction were calculated by SUPCRT92b, with thermodynamic properties of vivianite from
249 Al-Borno and Tomson (1994).

250

251 **3. Results**

252 *3.1 Limitations on seafloor weathering of apatite*

253 In continental rocks, apatite is the primary P-hosting mineral for chemical weathering,
254 and detrital P, mainly as apatite, is the predominant component of continental P input to the
255 ocean system (Compton et al., 2000; Ruttenberg et al., 2014). In oceanic crust, apatite is
256 unlikely to be a major host mineral for P due to high saturation concentrations; rather P is
257 expected to exist either as trace impurities in silicate minerals — including olivine,
258 clinopyroxene, and plagioclase — or in basaltic glass (Brunet & Chazot, 2001). However,
259 trace amounts of apatite are common in basalts and gabbros (e.g., Anderson & Greenland,
260 1969; Coogan et al., 2001; Meurer & Natland, 2001), and apatite may precipitate locally due
261 to the P gradient near a growing crystal (Green & Watson, 1982).

262 If the concentration of dissolved P in the weathering fluid reaches the solubility limit
263 of apatite, apatite as the reactant will have no reaction affinity to dissolve further (Brantley
264 and Olsen, 2014). Salinity and pH are the two most important environmental determinants of

apatite solubility. Seawater pH is primarily buffered by the riverine transport of alkalinity, seafloor weathering of silicates, and hydrothermal fluids. Although the Archean atmosphere had high $pCO_{2,g}$, simulated pH of Archean seawater ranges from 6.5 to 7.0 (Halevy and Bachan, 2017; Krissansen-Totton et al., 2018), unlike the more acidic rainwater that drove continental weathering (Hao et al., 2017). Ca^{2+} level is another important factor in determining the solubility of P. It has been proposed that Archean seawater was more enriched in Ca^{2+} than the modern oceans because of enhanced hydrothermal alteration of the seafloor (Halevy and Bachan, 2017; Jones et al., 2015; Krissansen-Totton et al., 2018).

Based on these considerations, and applying our additional assumptions for Archean seawater composition (**Methods**), we calculated the solubility limits for three common types of apatite: Cl-apatite, F-apatite, and OH-apatite. **Fig. 1** shows that all three minerals had limited solubility (< 0.1 μM; predominantly as $H_2PO_4^-$ at pH < 7) in Archean seawater; results are consistent whether one assumes rapid or slow continental emergence on the late Archean Earth. The low solubility of apatite minerals in Archean seawater contrasts markedly with their high solubilities in contemporaneous continental weathering fluids (Hao et al., 2017), a difference primarily ascribed to the higher pH and higher concentrations of Ca^{2+} and halogens in Archean seawater, relative to rain or river water (Hao et al., 2020). In addition, the log dissolution rate of apatite minerals decreases linearly with increasing pH in acidic water (Brantley and Olsen, 2014; Guidry and Mackenzie, 2003). Thus, in Archean oceans, the weathering of apatite was both thermodynamically and kinetically less favorable than continental weathering. Indeed, the direct implication of **Fig. 1** is that seafloor weathering of apatite minerals could have contributed little if any P to early marine life. Consistent with these simulation results, we observed detrital apatite as the major P-phase in Archean black shales, with tiny overgrowths of secondary apatite (Bothaville Formation, South Africa; ca. 2700 Ma) (Fig. 7a & b). Bothaville sediments reflect rapid uplift and erosion of a crustal bloc

290 to the west (Schneiderhan et al., 2011), resulting in large input of P with a major proportion
291 being detrital apatite minerals (Hao et al., 2020). In addition, as discussed in *Sec. 4.1*, we
292 think that seafloor weathering of basalt would contribute little P to early oceans.
293
294 *3.2 Solubility and precipitation of secondary phosphates in the Archean seawater*
295 On the modern Earth, seafloor weathering serves as a net sink for P that balances
296 continental input (Compton et al., 2010), with P removal occurring mainly as organic-P,
297 various authigenic/biogenic phosphate minerals (CFA, HAP, and other phosphates), and
298 surface adsorption onto or co-precipitation with Fe(III)-(hydr)oxide and carbonate
299 (Ruttenberg et al., 2014). In anoxic Archean seawater, Fe(II) oxidation could and did occur
300 via photo- and/or bio-oxidation of Fe(II), or the cooling of hydrothermal fluids, as
301 documented by ferric iron in Archean banded iron formations. Several investigators analyzed
302 the P content in BIFs in order to reconstruct paleo-concentrations of P, assuming that
303 adsorption onto Fe-(hydr)oxide was the major sink for P (Jones et al., 2015; Konhauser et al.,
304 2007; Planavsky et al., 2010).
305 In addition to surface adsorption, however, our simulations suggest that vivianite
306 would have a much lower solubility in Archean seawater than other secondary P-minerals
307 (e.g. octacalcium phosphate, or OCP) (**Table S1** and **Fig. 2**). Assuming a moderate
308 supersaturation state of vivianite, Ω = 100 or 1000, our calculations indicate that phosphate
309 solubility in Archean oceans would have been similar to that estimated by Jones et al. (2015),
310 0.1 to 0.3 μM dissolved phosphate depending on Ω and age (**Fig. 2**). This estimate depends
311 heavily on the feasibility of vivianite precipitation, experimentally shown to be sluggish at
312 low supersaturation but potentially facilitated by microbial reduction and mineral adsorption
313 in natural systems (Sec. *4.2*). Regardless, in the low-P Archean seawater, octacalcium
314 phosphate (OCP) as the precursor phase of marine apatite (Van Cappellen, 1991) has no

thermodynamic affinity to precipitate. Undersaturation of OCP in the Archean seawater further indicates that, precipitation of apatite minerals, although thermodynamically favorable given their extremely low solubilities (**Fig. 1**), was not kinetically feasible (Gunnars et al., 2004).

Using the reported crystallization kinetics of vivianite (Madsen & Hansen, 2014; Madsen, 2019) and assuming the presence of mineral seed, we estimated 46-695 μm crystal growth for 1 year at supersaturation states of 100-1000 in the Archean seawater (**Fig. 3a**; assuming 0.1 to 1 mM Fe^{2+}), this falling into the size range of vivianite nodules found in natural sediments at low supersaturation states (Rothe et al., 2016). Following the method proposed by Derry (2015), we calculated the precipitation rate of vivianite from water column to sediment, showing that the depositional flux of P as vivianite in the Archean oceans could easily have reached levels comparable to the modern sinking flux for P at $\Omega >$ 10 (i.e., solubility of P = 0.03 μM) (**Fig. 3b**). Derry's model assumes ready vivianite precipitation even at low supersaturation states, but the actual precipitation flux should depend heavily on precipitation kinetics of vivianite, which is known to be affected by a number of factors (Sec. *4.2*).

3.3 Post-depositional transformation of vivianite

As discussed above, vivianite precipitation could be an important P sink in Archean oceans. The fate of vivianite during diagenesis and metamorphism, however, requires consideration.

Assuming that siderite and greenalite precipitation could reach in equilibrium, our simulations show that in the porewater environment siderite solubility is 2 to 4 orders of magnitude lower than greenalite (**Fig. 4a & S3a**). Therefore, if siderite precipitation becomes kinetically feasible during burial diagenesis (Sec. *4.3*), it should limit the solubility of Fe(II)

to low values, as argued for Archean porewaters (Tosca et al., 2019). Under these conditions, vivianite becomes much more soluble than other secondary phosphate minerals, e.g. octacalcium phosphate (OCP) and carbonate fluorapatite (francolite) (**Fig. 4b & S3b**). OCP is thought to be the precursor phase of marine apatite minerals (Eanes & Meyer, 1977; Van Cappellen, 1991). In the modern marine sediments, precipitation of P as apatite minerals is thought to one major P sink in the long run (Ruttenberg, 2014; Van Cappellen, 1991). Our simulations show that in the Archean porewaters, the solubilities of apatite minerals are expected to be extremely low (at least 1-3 orders of magnitude lower than OCP and 5-9 orders of magnitude lower than vivianite; **Fig. 4c**), implying strong thermodynamic affinity for the transformation from vivianite to OCP and apatite minerals (*Sec 4.3*).

In addition, we calculated the reaction constant for the transformation of vivianite + calcite (+ fluorite; with a fluorine level similar to the seawater) to F-apatite + siderite (with release of water) at elevated temperatures, mimicking the burial diagenesis and low-grade metamorphism of vivianite. The result suggests that log (reaction constant) is >> 1, and its value increases with temperature (**Fig. 5**), suggesting that the transformation becomes thermodynamically more and more favorable. Therefore, it can be reasonably expected that at the elevated temperatures of burial diagenesis and metamorphism (> 100 °C, where the precipitation kinetics of apatite and siderite are feasible), vivianite would inevitably transform to apatite.

3.3 Total phosphorus for Archean primary production

Fig. 6 shows the proportional contribution of continental weathering to the total P requirement for NPP as a function of recycling efficiency. In line with the hypothesis by Laakso & Schrag (2018), the figure indicates that on the Archean Earth, continental weathering would provide the major source of P for life in photic zone, unlike today. Based

365 on our estimate of continental P flux (**Table 1**) and a recycling efficiency of 0.78 (Sec. *4.4*),
366 we calculate the recycling flux of organic P by the end of the Archean Eon to have been 14-
367 120 $\times$ 10^{10} moles P/yr (**Table 1**). Note that the flux of recycling P, which represents an
368 optimistic estimate in this study, depends heavily on the recycling efficiency (and thus burial
369 efficiency) of organic matter in the Archean Eon, which is poorly constrained (Kipp et al.,
370 2019) and might have evolved through time (Sec. *4.4*). Assuming deep water P
371 concentrations equivalent to 10% of the modern value and a typical vertical mixing rate (3
372 m/yr), Ward et al. (2019) recently estimated Archean P recycling to have been 40 $\times$ 10^{10}
373 moles P/yr, within the range of our values. Regardless of uncertainties, these estimates agree
374 that the recycling flux of P in late Archean oceans was 1-2 orders of magnitude lower than
375 today's (about 3710 $\times$ 10^{10} moles P/yr; Schlesinger and Bernhardt, 2013). Together with our
376 estimated continental input of P, up to 18-154 $\times$ 10^{10} moles P/yr would have been available
377 for marine primary productivity by the end of Archean Eon, 0.5-4% of modern values (**Table**
378 **1**). Because of limited continental emergence and elevation, the continental flux of P and thus
379 the recycling flux of P would have been much smaller on the earlier Archean Earth, perhaps
380 $<$ 0.05 $\times$ 10^{10} moles P/yr, i.e. 0.001 % of the modern value (**Table 1**).
381
382 **4. Discussion**
383 *4.1 Seafloor weathering of phosphorus*
384 In the modern ocean, seafloor weathering is widely agreed to be a net sink for P,
385 primarily due to surface adsorption onto Fe(III)-hydroxide or carbonate (Wheat et al., 1996)
386 or (co)precipitation of P-minerals (hydroxylapatite, CAP, REE/Al-phosphates) (Ruttenberg et
387 al., 2014). Given the reducing and weakly acidic nature of Archean seawater, however,
388 dissolution of basaltic glass has been proposed as a source of P for autotrophs (Kakegawa,
389 2003). To date, there is limited evidence to support this hypothesis. Syverson et al. (2020)

recently observed slight P release during alteration of basalt at 25 °C under anoxic conditions, whereas alteration experiments under oxic condition did not show any P release. These observations seemingly support seafloor weathering as a potential source of P in the anoxic Archean ocean(s). However, Syverson et al. used a simulated seawater solution without any inorganic C, which diverges markedly from realistic estimates of Archean seawater chemistry (high $CO_{2,aq}$ and (bi)carbonate species; Halevy & Bachan, 2017; Krissansen-Totton et al., 2018). Under these more realistic conditions, seafloor weathering would precipitate abundant carbonate minerals, a major sink in the Archean carbon cycle (Krissansen-Totton et al., 2018) as well as a known mineral product in modern seafloor weathering. Carbonate minerals have a strong affinity to phosphate and could limit soluble P by either surface adsorption (de Kanel & Morse, 1978; Millero et al., 2001; Wheat et al., 1996) or co-precipitation as carbonate apatite (Freeman & Rowell, 1981; Rubinstein et al., 2012; Xu et al., 2014); both represent a major sink for P in modern carbonate-rich and/or anoxic sediments (e.g. Baturin, 2003; Fourqurean et al., 1992; Kraal et al., 2017). In addition, elevated temperature or presence of divalent cations (e.g. Ca^{2+}, Mg^{2+}) would increase uptake of phosphate by carbonate (Millero et al., 2001). In fact, carbonate minerals can capture 2.3 – 4.5 * 10^{12} mole P/yr in the modern ocean, 2 - 4 times the sink provided by hydrothermal iron hydroxides (Baturin, 2003); carbonates could be expected to form a larger sink in the Archean due to higher $pCO_{2,g}$ and highly weatherable rocks.

In another study, Murakami et al. (2019) investigated the hydrothermal alteration of basalt under CO_2-rich condition (+ 30 mmole/kg Ca^{2+}), mimicking Archean atmospheric and seawater composition. Their experiments revealed under high CO_2 conditions, carbonate was a major alteration product, with higher P-uptake than occurred in a CO_2-free run, supporting the hypothesis that carbonate minerals would take up phosphate released from seafloor weathering or via diffusion from seawater. A limited contribution of P from glass weathering

415 is further supported by the observations of modern and Archean glasses altered under anoxic
416 conditions; these showed enrichment or no loss of P (Alt & Honnorez, 1984; Rubinstein et al.,
417 2012; Staudigel et al., 2008). In addition to uptake by carbonates, there are other substantial
418 sinks of P during seafloor weathering, including the precipitation of Al/REE phosphates
419 (Byrne & Kim, 1993; Rasmussen, 2000) and vivianite (this study; Derry et al., 2015). Based
420 on the above considerations, we argue that seafloor weathering should be a negligible source
421 and possibly a large sink in the Archean P cycle.
422
423 *4.2 Vivianite precipitation kinetics*
424 Direct precipitation of vivianite from Fe(II)-PO_4 solution has been experimentally
425 shown to be kinetically inhibited at low saturation states under ambient conditions
426 (Walpersdorf et al., 2013). In addition, at low supersaturation states, vivianite precipitation
427 has been shown to follow spiral growth mechanism, at rates slower than surface-nucleation
428 growth at high supersaturation states (Madsen & Hansen, 2014; Madsen, 2019). Altogether,
429 slow kinetics of precipitation and crystallization might indicate a relatively minor role for
430 vivianite as a P sink in Archean oceans. Indeed, Johnson et al. (2020) suggested that vivianite
431 was not a major P sink in the ferruginous sediments of the Mesoproterozoic Sherwin
432 Ironstone despite the high supersaturation states predicted by thermodynamic models.
433 However, in modern Fe(II)-rich anoxic waters (Cosmidis et al., 2014) and sediments (Borch
434 & Fendorf, 2008; Jilbert & Slomp, 2013; Sánchez-Román et al. 2015), vivianite precipitation
435 can be facilitated by microbial reduction of Fe(III) in presence of phosphate. In addition,
436 phosphate adsorbed into ferrous minerals, e.g. green rust, has been shown to quickly
437 transform into vivianite (Hansen & Poulsen, 1999; Xiong et al., 2019). The presence of
438 mineral seeds (e.g. quartz) could also facilitate the crystallization of vivianite and lower the
439 supersaturation demand (Liu et al., 2018). These mechanisms may explain the precipitation

of vivianite at low to moderate supersaturation states in modern anoxic waters (Ω = 40 for lake Pavin; Cosmidis et al., 2014) and sediments (Ω < 1 for Baltic Sea porewater; Jilbert & Slomp, 2013; Ω < 1000 for Lake Groß-Glienicke and Lake Arendsee porewaters, although Lake Spitzingsee porewater vivianite is absent at Ω > 10000; Rothe et al., 2016), which might also have been true for Archean oceans.

Given these uncertainties, we cannot provide a quantitative estimate for the sedimentation flux of phosphate as vivianite in Archean oceans and thus evaluate the importance of vivianite precipitation as a P sink. Global vivianite fluxes would be greatly affected by poorly constrained concentrations and fluxes of phosphate and ferrous iron in Archean seawater. Moreover, the precipitation kinetics of vivianite are strongly influenced by temperature (Madsen & Hansen, 2014), microbial activity (Borch & Fendorf, 2008), and mineral surface (Hansen & Poulsen, 1999; Liu et al., 2018; Xiong et al., 2019). Additionally, adsorption onto Fe-(hydr)oxide (Bjerrum and Canfield, 2002; Jones et al., 2015) or green rust (Zegeye et al., 2012) and/or co-precipitation as Fe(III)-phosphate would have competed for P with vivianite precipitation in surface seawater, and these processes cannot be quantified on the basis of available information. Nevertheless, we support the qualitative argument that the global flux of P precipitated by vivianite was important in the Archean P cycle, limited largely by the input of P from continental weathering and riverine transport (**Table 1**).

4.3 Burial of P in the Archean marine sediments

Within sediments, precipitation of siderite could become kinetically feasible during diagenesis through bioreduction of Fe(III) in the presence of organic matter (Vuillemin et al., 2019) or via burial heating. Our simulations suggest that siderite precipitation would minimize the solubility of Fe(II) (**Fig. 4a**); as a result, sedimentary vivianite would have higher solubility than calcium phosphates (**Fig. 4b & 4c**). Under these circumstances,

vivianite becomes unstable with respect to calcium phosphates, and the dissolution of vivianite could result in higher P than OCP and francolite solubility in porewater (Thinnappan et al., 2008), inducing OCP or francolite precipitation. OCP has been suggested as essential precursor phase for apatite precipitation (Gunnars et al., 2004; Van Cappellen, 1991) and the presence of OCP could facilitate the precipitation of apatite, which would continue until P levels declined to values lower than OCP solubility (Nancollas, 1984; Van Cappellen, 1991). Given the much lower solubility of apatite minerals than vivianite and OCP (**Fig. 4c**), precipitation of apatite should be a significant P-sink, maintaining low levels of P in Archean porewater (< 1 μM as the solubility of OCP in **Fig. 4b**).

Other forms of deposited P, including Fe(III)/Al-hydroxide or carbonate bound- and organic-P, might also transform into calcium phosphates, along with the reduction of Fe(III) and breakdown of organic matter in porewater environments. Indeed, transformation of Al/Fe(III)-bound P to OCP has been observed in modern nearshore sediments and shown to be facilitated by increasing pH and/or decreasing Eh (Oxmann & Schwendenmann, 2015). In modern anoxic sediment, it has been observed that organic-P could transform progressively into calcium phosphate with the aid of $CaCO_3$ during burial diagenesis (Kraal et al., 2017). Archean porewaters were probably enriched in Ca (**Fig. S1-2**) and enhanced seafloor weathering at high $pCO_{2,g}$ would induce widespread precipitation of $CaCO_3$ in sediments (Sleep & Zahnle, 2001). Thus, as argued for vivianite, organic-P would also transform into calcium phosphates during burial diagenesis, depending on the relative concentrations of Ca^{2+} and Fe^{2+} and ambient pH in sediments. Recently, Johnson et al. (2020) reported carbonate fluorapatite as the major phosphate in a Mesoproterozoic ferruginous sediment, probably transformed from Fe(III)-bound or organic P during burial diagenesis, supporting the hypothesis that precipitation of calcium phosphates as the dominant long-term P-sink.

We also note that the present day mineralogy of iron formations is thought to bear the strong imprint of diagenesis, including supergene enrichment (Rasmussen et al., 2016). Therefore, the current Fe and P mineralogy of Archean BIFs may not provide a strong test of our or any other low-temperature environmental hypotheses. Ca-rich carbonate would be a major product of seafloor weathering under a high $pCO_{2,g}$ Archean atmosphere (Sleep and Zahnle, 2001), its solubility increasing with rising burial pressure. $CaCO_3$ dissolution has been shown to aid long-term sequestration of P in the sediments of modern anoxic basins by facilitating the precipitation of Ca-P minerals (Kraal et al., 2017; Krajewski et al., 1994). Therefore, in the long term, progressive burial might have converted vivianite to less soluble apatite.

Consistent with these considerations, tiny spheroids of apatite (**Fig. 7**) have been observed in Archean and Proterozoic carbonaceous shales (several % TOC) from multiple and widely separated localities. These spheroids typically measure 2 to 5 micrometers in diameter and may form solid spheres as well as thick- or thin-walled shells (**Fig. 7**). The illustrated Archean example (Bothaville Formation, South Africa; ca. 2700 Ma) shows predominantly detrital grains with small later diagenetic overgrowths (**Fig. 7a-b**). In essence, this coexistence suggests that apatite was originally deposited as a detrital component from continental erosion; in places where P concentrations reached saturation for apatite overgrowth, diagenetic overgrowths started to fill in adjacent pore space. In contrast to the Archean samples, common to all of the Proterozoic precipitates are micron-sized spheres or shells that consist of radiating apatite crystals that in places may extend beyond the apparent original sphere or shell margin outline (**Fig. 7c-f**). Thin-walled shells commonly show variable degrees of deformation, suggesting that apatite nucleated on partially degraded cell walls or extracellular envelopes. In places, multiple spheres are joined together to form a single mineralized entity (Schieber et al., 2007). The clustering of spheroids (**Fig. 7c, d, e**),

514 the apparent progression from mineralized membranes, to thick-walled shells and solid
515 spheres (**Fig. 7f**), and the commonly observed association with organic matter are suggestive
516 of an organic origin, possibly as mineralized microbes that were associated with decaying
517 organic matter (Schieber et al., 2007).

518 The microspheres are consistent with P liberation during organic remineralization,
519 followed by vivianite/OCP precipitation and, later, eventually transformation to apatite
520 during diagenesis, although we cannot reject the alternate possibility that phosphorus
521 precipitated originally as apatite. In either case, however, P liberated by organic
522 remineralization did not return to the water column, but rather was immobilized by mineral
523 precipitation.

524 In recent experiments, Herschy et al. (2018) documented the partial reduction of
525 orthophosphate (PO_4^{3-}) into phosphite (PO_3^{3-}) by Fe(II) at 180 °C, mimicking burial
526 diagenesis. This mechanism is possible, but it has little influence on our conclusions, as even
527 under favorable conditions only about 5% of precipitated phosphate would be reduced to
528 phosphite (Herschy et al., 2018). We note as well that the research in question did not include
529 Ca (either aqueous species or carbonate) in the experimental system. Ca would significantly
530 favor the stability of apatite $Ca_5(PO_3)_3(OH,F,Cl)$ against reduction of orthophosphate at the
531 elevated temperatures and pressures associated with diagenesis and low-grade metamorphism
532 (**Fig. 5**). This inference is consistent with evidence that apatite is the dominant P-mineral in
533 ancient sedimentary rocks (Friend et al., 2008; Lepland et al., 2002).

534

535 *4.4 Recycling of P in the Archean ocean*

536 In the modern ocean, continental input of bioavailable P accounts for less than 1% of
537 the P requirement for net primary production (NPP) (**Table 1**; Schlesinger & Bernhardt,
538 2013); the recycling of biological phosphate within the ocean overwhelmingly dominates P

539 supply to the photic zone. On the Archean Earth, however, when the atmosphere and oceans
540 were largely reducing, a lack of oxidants would have suppressed the recycling efficiency of
541 biological P (Kipp and Stüeken, 2017). And, as already introduced, our simulation shows that
542 precipitation of secondary phosphates as vivianite or Ca-phosphates might also maintain low
543 concentrations of dissolved P in Archean seawater and porewater, impeding the recycling of
544 phosphate freed via organic matter remineralization. Therefore, the recycling of biological P
545 was very likely much weaker in Archean oceans and, accordingly, NPP must have been much
546 lower.

547 The recycling efficiency of organic matter is inversely proportional to the burial
548 efficiency of NPP, which depends on the availability of oxygen (Hedges et al., 1999) and
549 other oxidants, as well as bioturbation (Zonneveld et al., 2010). Indeed, burial efficiency has
550 an inverse relationship with exposure of oxygen (as well as other oxidants), and extrapolation
551 of the correlation to zero oxygen exposure results in 40-50% burial efficiency (Hartnett et al.,
552 1998). Moreover, it has been estimated that burial efficiency can be as high as 22-32% in
553 modern ferruginous lakes (Crowe et al., 2011; Katsev & Crowe, 2015, Kuntz et al., 2015),
554 although transferring this estimate to the entire ocean needs further investigation. In contrast,
555 the burial efficiency of oceanic NPP is about 0.1% in modern oceans (Hedges and Keil, 1995)

556 Modern lakes certainly have greater inventories of oxidants (O_2, SO_4^{2-}, NO_3^-) than
557 Archean seawater. Input of sulfate would also undermine the burial P as vivianite by lowering
558 the solubility of Fe(II) in anoxic waters and sediments (Rothe et al., 2015); however, the Archean
559 seawater was depleted in sulfate (Lyons & Gill, 2010). Such considerations suggest that the
560 recycling efficiency of biological P would have been even lower in Archean oceans than in
561 modern ferruginous lakes, i.e. $R_{recycling}$ < 0.68-0.78 in the Archean (**Fig. 6**). As noted above,
562 an independent approach by Ward et al. (2019) resulted in similar estimate for the flux of

563 recycled P toward the end of the Archean, supporting a lower recycling efficiency of P than
564 the modern value (~0.997).

565 Recently, Kipp & Stueken (2017) compiled the availability of oxidants for recycling P
566 through Earth history and used these to argue that rates of P recycling in Archean seawater
567 were 100 times lower than the modern, i.e., a recycling efficiency < 0.01. Kipp & Stueken's
568 estimate should represent a lower limit of recycling efficiency, considering the preferential
569 release of P during organic decomposition (Clark et al., 1998) and photo-oxidation of
570 organics in surface seawater (see below). Moreover the absence of zooplankton and fecal
571 pellets in the Archean ocean might have led to less efficient deposition of particulate organic
572 carbon (Logan et al., 1995) and, consequently, burial of organic matter in the Archean ocean.

573 It is also important to ask whether the recycling efficiency of nutrients might have
574 evolved through Archean time as a function of the redox state of surface environments (Hao
575 et al., 2019) and continental emergence (thus, shelf area for upwelling; see Olson et al., 2019).
576 In the early Archean, when surface environments were more reducing and emergent
577 continents were minimal, recycling of organic matter would be severely depressed due to
578 oxidant limitation and limited shelf area for upwelling. However, in the middle to late
579 Archean, oxidant inventories increased (Stueken et al., 2012) and continental lands
580 increasingly emerged above sea level (Flament et al., 2013; Korenaga et al., 2017). Back
581 reduction of river-transported sulfate might have depleted dissolved seawater Fe(II)
582 regionally, even generating euxinic areas in the late Archean ocean (Reinhard et al., 2009).
583 The solubility of vivianite would increase significantly in regionally euxinic zones,
584 engendering a simultaneous increase of P solubility. As a consequence, the recycling
585 efficiency of nutrients would be expected to increase.

586 In modern surface seawater, dissolved organic P (DOP) can reach significant levels,
587 sometimes even higher than dissolved inorganic P (Ruttenberg. 2014). Due to the high

588 stability of biomolecules under reducing conditions, organic P might have also been
589 important in the Archean seawater. However, experimental studies have suggested that the
590 lifetime of organic-P under UV radiation would be short (Francko & Heath, 1979). Thus,
591 high UV radiation, due to the lack of an Archean ozone shield, might efficiently destroy
592 organic P in the surface layers of Archean seawater. Therefore, dissolved organic P might
593 have played a relatively minor role for the Archean life in photic zone.
594
595 *4.5 Electron vs. phosphorus limitation on Archean primary production?*
596 How do the simulations presented here inform the debate about nutrient versus
597 electron donor limitation on net primary production (NPP) in Archean oceans? Total fluxes
598 of electron donors on the Archean Earth have been proposed in several studies (Canfield et
599 al., 2006; Kharecha et al., 2005; Ward et al., 2019), but estimated values vary markedly (**Fig.**
600 **8**). By comparison, fluxes of nutrients have been less commonly investigated (Laakso and
601 Schrag, 2018; Ward et al., 2019), particularly for phosphorus, thought to be the most
602 probable limiting nutrient. [It has been proposed that nitrogen limits global primary
603 production on geologic time scales (Falkowski, 1997), but at the low levels for Archean NPP
604 advocated here, nitrogen demand could have been met by modest rates of biological nitrogen
605 fixation, and, especially during the early Archean, might have been sustained in most times
606 and in many places by abiotic N-fixation (Chameides and Walker, 1981; Ward et al., 2019;
607 Wong et al., 2017).]
608 Various lines of evidence support the concept of a more or less low-P Archean ocean
609 (Bjerrum and Canfield, 2002; Jones et al., 2015; Planavsky et al., 2010; Reinhard et al., 2017).
610 Here, we estimate that the total flux of P could have reached 18-154 $\times 10^{10}$ moles P/yr by the
611 end of the Archean Eon. Assuming a standard Redfield C:P of 106:1, this is equivalent to a
612 NPP of 19-163 $\times 10^{12}$ moles C/yr, or 0.5-4% of the modern value (ca. 4000 $\times 10^{12}$ moles C/yr;

613 Field et al., 1998). In the modern ocean, Redfield ratios of individual populations vary within
614 limits set by the fundamental biochemical composition of their constituent cells (Geider and
615 La Roche, 2002). If, following Laakso and Schrag (2018), we accept that mean C:P could
616 have reached values as high at 195:1, the total flux of P could have supported up to 7% of the
617 modern NPP by the end of the Archean Eon. This level of NPP is higher than the estimate by
618 Ward et al. (2019), i.e. < 0.1% for the late Archean time limited by the availability of electron
619 donors and the efficiency of anoxygenic photosynthesis.

620 We stress, however, that our estimated P flux varies markedly through a billion years
621 of recorded Archean history (Hao et al., 2020; **Figure 8**). Early in the Archean, when
622 continental weathering of P was severely limited by continental exposure and elevation, the
623 weathering and erosional flux of P from continents would have been extremely low (**Table 1**).
624 Because of this factor and limitations on recycling efficiency from both low oxidant supply
625 and the probability of P capture by vivianite, P supplied by recycling would also have been
626 extremely low (**Table 1**). Moreover, the limited area of emergent continents and, thus, coastal
627 continental margin shelf could result in relatively weak upwelling, and in consequence,
628 reduced nutrient recycling (Olson et al., 2019). P, then, could have limited NPP to less than
629 0.05×10^{12} moles C/yr, a factor of eight lower than Ward et al.'s estimate for an Archean
630 biosphere fueled by anoxygenic photosynthesis and far lower than the value estimated by
631 Canfield et al. (2006). Altogether, these results might indicate transition from a P-limited
632 biosphere in the early Archean to an electron donor-limited biosphere as continents emerged
633 toward the end of Archean (**Fig. 8**).

634 Questions of NPP limitation by P or electron donors are straightforward only in a
635 world without oxygenic photosynthesis. Once bacteria evolved the capacity to split water, the
636 supply of electron donors became essentially unlimited and primary production would,
637 forever after, be limited by nutrient availability, primarily phosphorus (Tyrrell et al., 1999).

Despite continuing debate about when oxygenic photosynthesis first evolved, there is a consensus that the oxygenation of atmosphere at 2.4 Ga required oxygenic photosynthesis. Ward et al. (2016) simulated the oxygenation time of the Archean atmosphere under a series of settings (primary production, burial fraction, and methanogenic fraction) and suggested that with a primary production of 10^{14} moles C/yr, irreversible oxygenation of atmosphere would happen within ~ 100 kyr. This level of primary production falls into the range of NPP supported by our estimation of total P in the end of Archean Eon (**Table 1**). Therefore, increasing emergence of continents and riverine transport of phosphorus would lead to higher primary productivity and once oxygenic autotrophs attained ecological prominence, rapid oxygenation of atmosphere as the Proterozoic Eon began.

5. Conclusions

The total flux of P for marine ecosystems predominantly reflects input from continental weathering and the recycling of P within the ocean. Archean seawater was anoxic, with a limited supply of oxidants, suppressing P recycling and so linking primary production more closely to continental weathering. Although Archean seawater was weakly acidic, apatite solubility would have been very low due to high levels of Ca and halogens; for this reason, seafloor weathering of P should not have been a major source of P for Archean marine ecosystems. In addition, the solubility of vivianite is predicted to have remained very low (0.1 to 0.3 μM) at moderate supersaturation states (Q/K = 100 to 1000) in Archean ferruginous seawater. Under these conditions, the precipitation flux of vivianite could have reached a level comparable to or higher than the modern sinking flux for P; therefore, it might have been a major sink in the Archean P cycle, with precipitation kinetically facilitated by microbial metabolism and mineral adsorption. Although potentially delivered to accumulating sediments, vivianite would not have been stable during burial diagenesis and

663 metamorphism, reacting readily with calcium carbonate to form more stably calcium
664 phosphates, particularly apatite.

665 Together with continental input of P, our current estimate of recycling P in the
666 Archean ocean would, under the most favorable circumstances, have allowed up to 7% of
667 modern NPP by the end of the Archean Eon. However, during the early and middle Archean,
668 inputs of continental weathering and P recycling would have been considerably weaker, and
669 the fluxes of electron donors higher. Therefore, NPP of the Archean marine ecosystems may
670 well have been limited by the availability of P instead of electron donors during most of the
671 Archean Eon. Indeed, on the early Archean Earth, NPP may well have been too low to
672 oxygenate the atmosphere and surface ocean, even if oxygenic photoautotrophs were widely
673 distributed in marine and fresh waters. Therefore, rapid oxygenation of the atmosphere might
674 only have become possible as increasing P fluxes from weathering and erosion increased near
675 the end of Archean Eon.

676

Acknowledgements We thank Dimitri A. Sverjensky, Cin-Ty Lee, Nicolas Coltice, Ciaran Harman, Mathew Pasek, Michael Kipp, David Catling, Lu Pan, Chao Liu, Liyan Tian, Ming Tang, Joshua Krissansen-Totton, Dustin Trail, and Paul Falkowski for helpful discussions. We also appreciate constructive comments by three anonymous reviewers, Nicolas Tosca, and Jeffrey Catalano. JHH & ID thank French National Research Agency (#ANR-15-CE31-0010), JHH & RMH thank NASA's Astrobiology Institute grant (80NSSC18M0093), and JHH, AHK, FH, and RMH thank W.M. Keck Foundation for financial support. RMH thanks the Templeton Foundation for financial support. JS thanks the sponsors of the Indiana University Shale Research Consortium (Anadarko, Chevron, ConocoPhillips, ExxonMobil, Shell, Equinor, Marathon, Whiting, and Wintershall) for support of the IU Shale Research Lab.

Author contributions JHH and AHK conceived of the project. JHH and FH performed the simulations; JHH and AHK analyzed the results. JS and AHK collected and investigated the textural mode of apatite grains in Archean and Proterozoic shales. All authors discussed the results and wrote the manuscript.

694 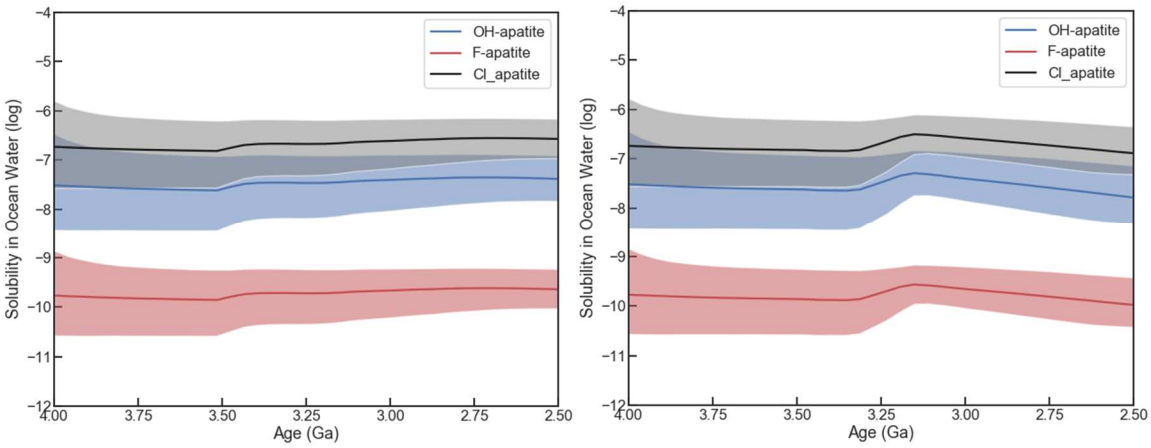

695 Figure 1. Limited solubilities of apatite minerals in the Archean seawater conditioned by the
696 model of a. slow continental emergence late in the Archean Eon (Flament et al., 2013); b.
697 rapid continental emergence late in the Archean Eon (Korenaga et al., 2017). Solid lines
698 show median outputs, and shaded regions show 95% confidence intervals.

699

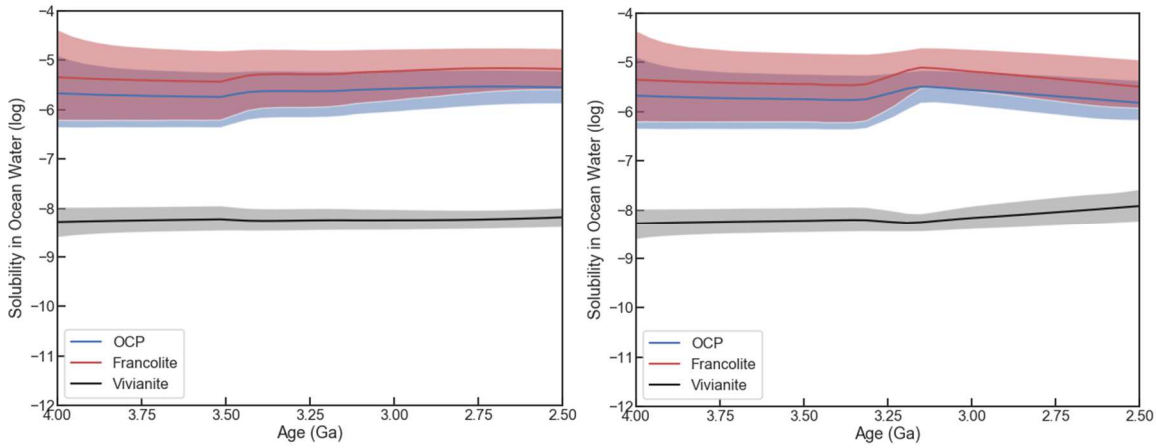

700

701 Figure 2. Solubilities of various secondary-P minerals in the Archean seawater conditioned
702 by the model of a. slow continental emergence late in the Archean Eon (Flament et al., 2013);
703 b. rapid continental emergence late in the Archean Eon (Korenaga et al., 2017). Solid lines
704 show median outputs, and shaded regions show 95% confidence intervals.

705

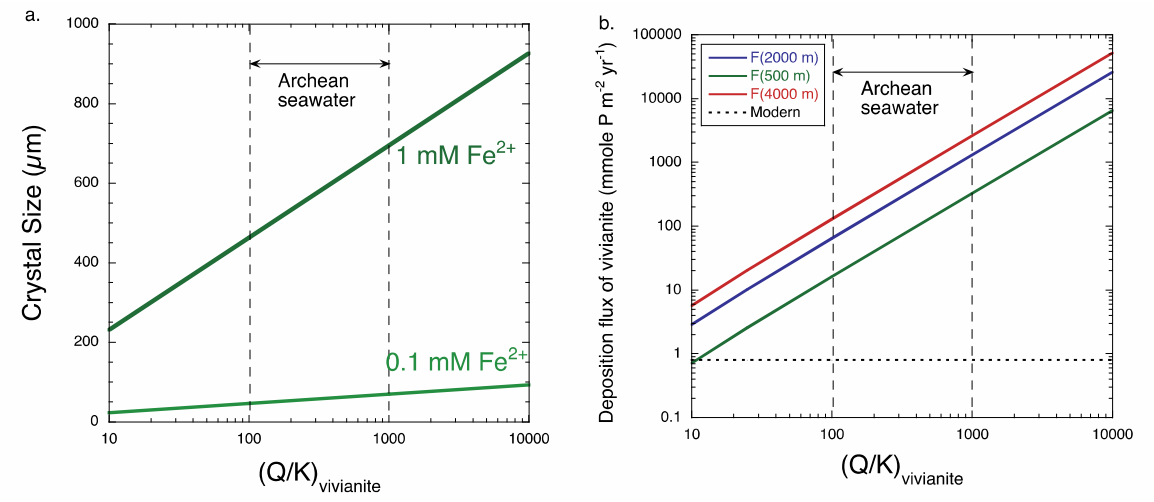

706

707 Figure 3. Precipitation of vivianite in Archean seawater: a. spiral growth (μm/yr) and b.
708 deposition flux of P as vivianite, as a log function of the probable range of supersaturation
709 states (*Q/K*) of vivianite and the thickness of the Archean ferruginous water column (colorful
710 lines in b). Dashed line in b shows the depositional flux of P in the modern ocean. Methods
711 adopted from Derry (2015).

712

713

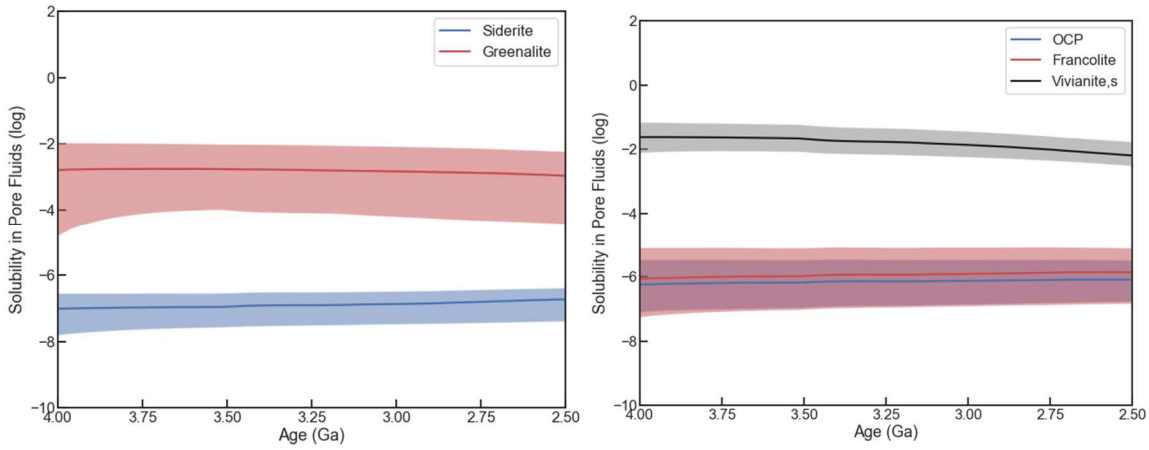

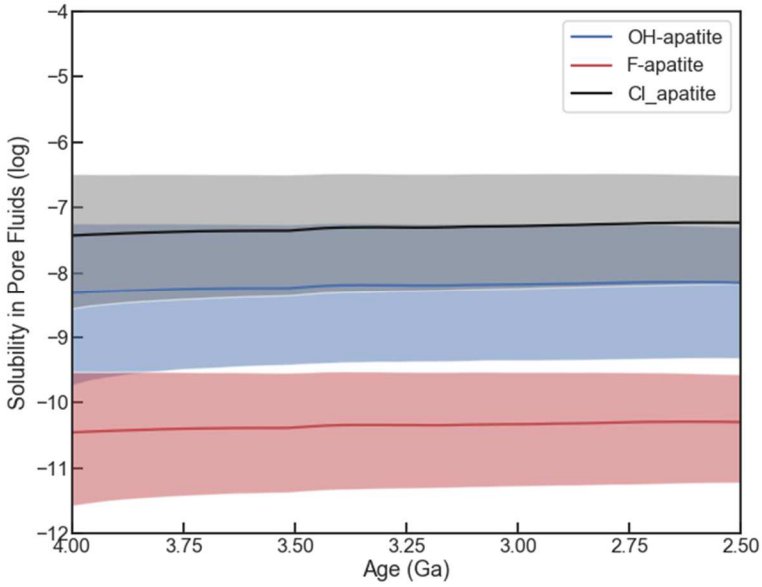

714

715 Figure 4. Solubility of siderite and greenalite (a), secondary phosphate minerals (b), and
716 apatite minerals (c) in porewater conditioned by the model of slow continental emergence in
717 the late Archean (Flament et al., 2013). The case of rapid continental emergence in the late
718 Archean (Korenaga et al., 2017) is shown as supplementary Fig. S3 with similar trajectories.
719 Solid lines show median outputs, and shaded regions show 95% confidence intervals.

720

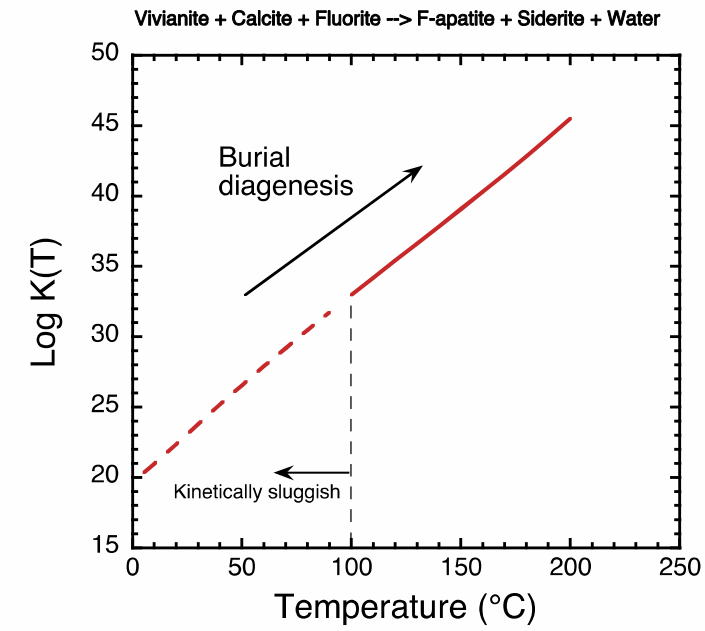

721

722 Figure 5. Transformation of vivianite into apatite during diagenesis and metamorphism:
723 equilibrium reaction constants of vivianite together with calcite and fluoride to form apatite
724 and siderite at elevated temperatures. Dashed red line indicates sluggish reaction kinetics due
725 to kinetic inhabitation of apatite and siderite precipitation at low temperatures.

726

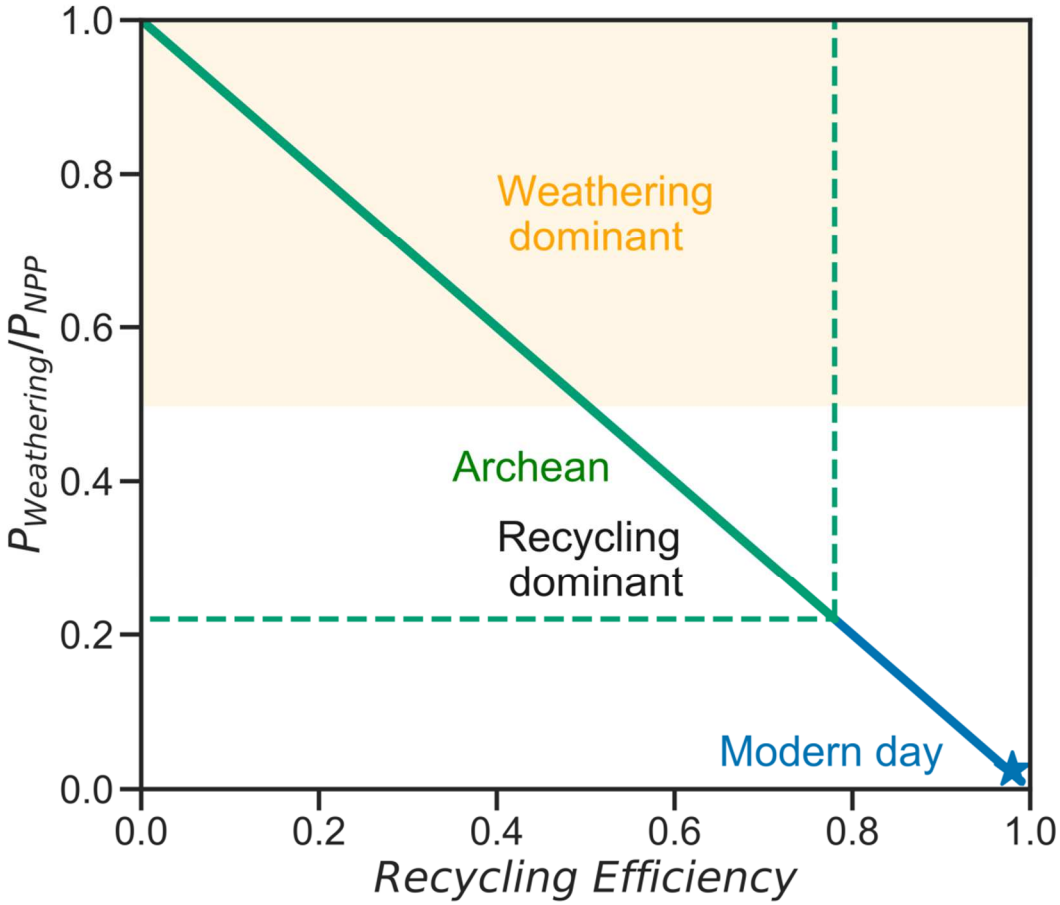

727

728 Figure 6. Proportional contribution of continental weathering flux to the total P requirement
729 of primary production plotted against recycling efficiency ($R_{recycling}$ = Recycling-P/Net
730 primary production P) of organic-P in seawater. Blue line indicates the range of modern
731 water bodies from anoxic lake ($R_{recycling}$ = in 0.78 in ferruginous Lake Matano; Crowe et al.
732 2011; Katsev & Crowe, 2015) to oxic seawater (star; $R_{recycling}$ = 0.998). The green line shows
733 our proposed Archean case ($0.01 < R_{recycling} < 0.78$; see Sec. *4.4* for discussion), in which P
734 recycling was limited within ferruginous water.

735

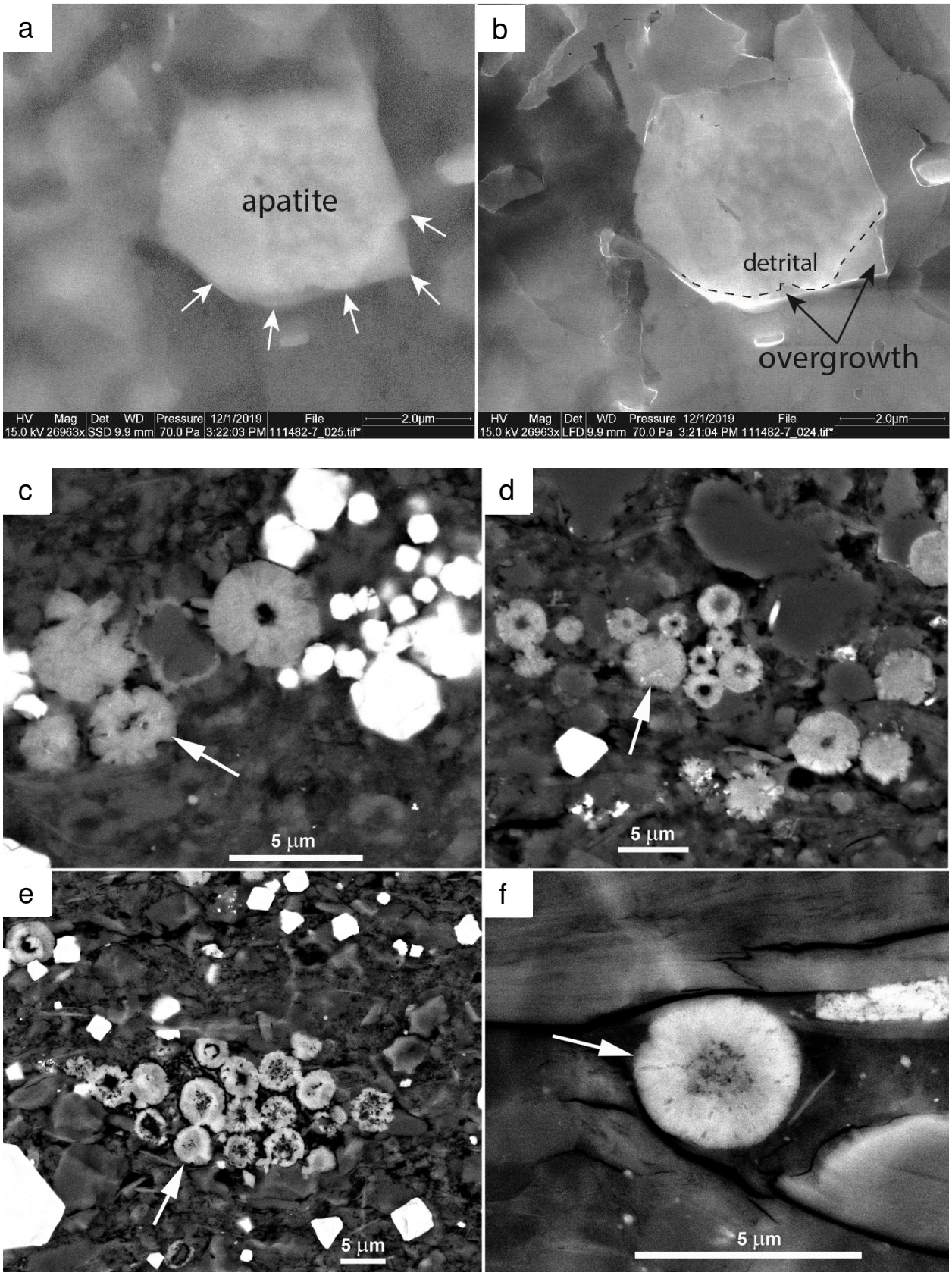

Figure 7. Contrasting appearance of apatite grains from Archean and Mesoproterozoic Archean and Mesoproterozoic carbonaceous shales as imaged by scanning electron

740 microscope (SEM). (a) Bothaville Formation (ca. 2700 Ma), South Africa, apatite grain in
741 center (white arrows), backscatter electron image. (b) Charge contrast in secondary electron
742 mode allows differentiation between detrital grain and diagenetic overgrowth (dashed line)
743 that extends into surrounding pore space. (c) Newland Formation (Belt Supergroup, Montana,
744 USA). Note deformed thin-walled “sphere” in center of image, as well as apatite crystals
745 projecting beyond sphere outlines. (d) Bijaigarh Shale, Vindhyan Supergroup, India, with
746 some deformed shells and apatite crystals projecting beyond sphere outlines. (e) Velkerri
747 Formation, Roper Group, Australia; note deformed thin-walled “spheres”. (f) Solid sphere
748 with less mineralized center portion, Kaltinsky Formation Siberia. With exception of image
749 (b), all images were acquired with a scanning electron microscope (SEM) in backscatter
750 mode.
751

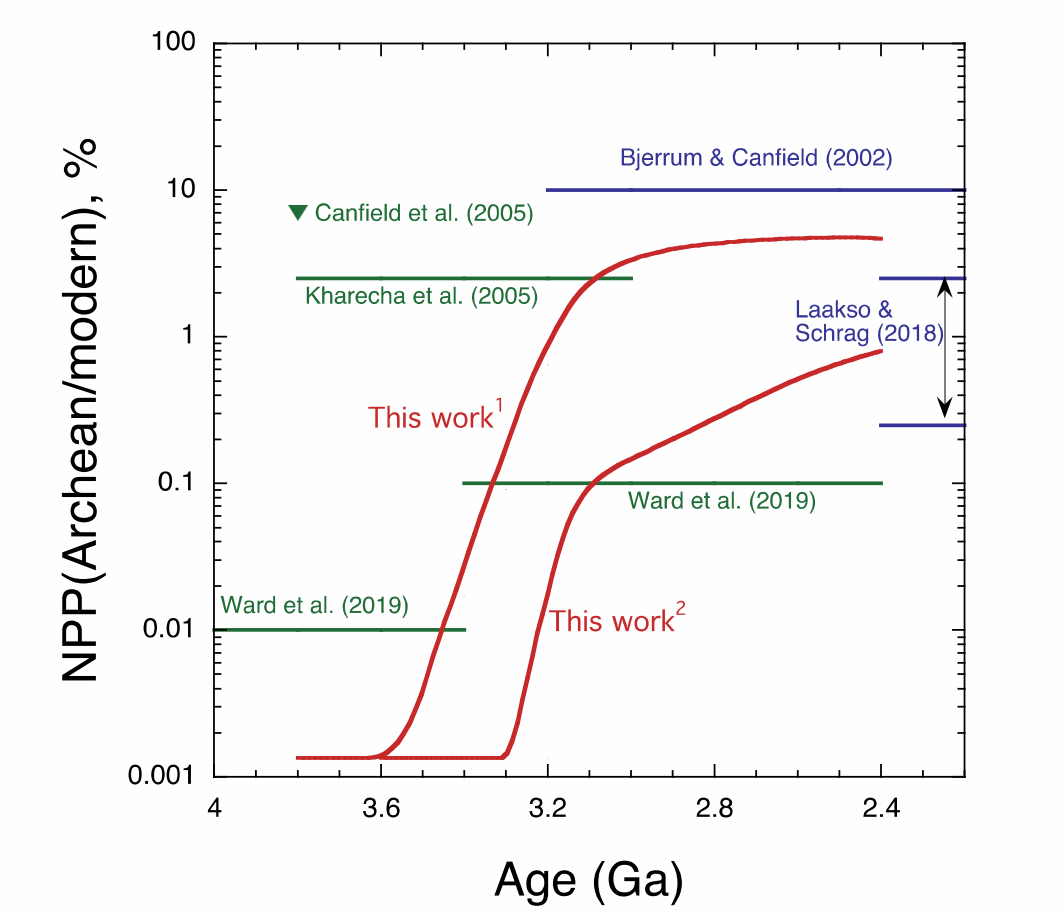

Figure 8. Upper limits of net primary production (NPP) in the ocean through the Archean Eon relative to the modern level. Blue lines show the previously reported constraints (upper limit or range) of NPP by the supply of P (Bjerrum & Canfield, 2002; Laakso & Schrag, 2018). Green lines display the previously reported constraints (upper limits) of NPP by the supply of electron donors (Canfield et al., 2005; Kharecha et al., 2005; Ward et al., 2019) and efficiency of early metabolisms (Ward et al., 2019). Red curves present our reconstructed evolution (upper limits) of NPP limited by the supply of P assuming: (1) slow emergence of land in the late Archean (Flament et al., 2013); (2) rapid emergence of land in the late Archean (Korenaga et al, 2017).

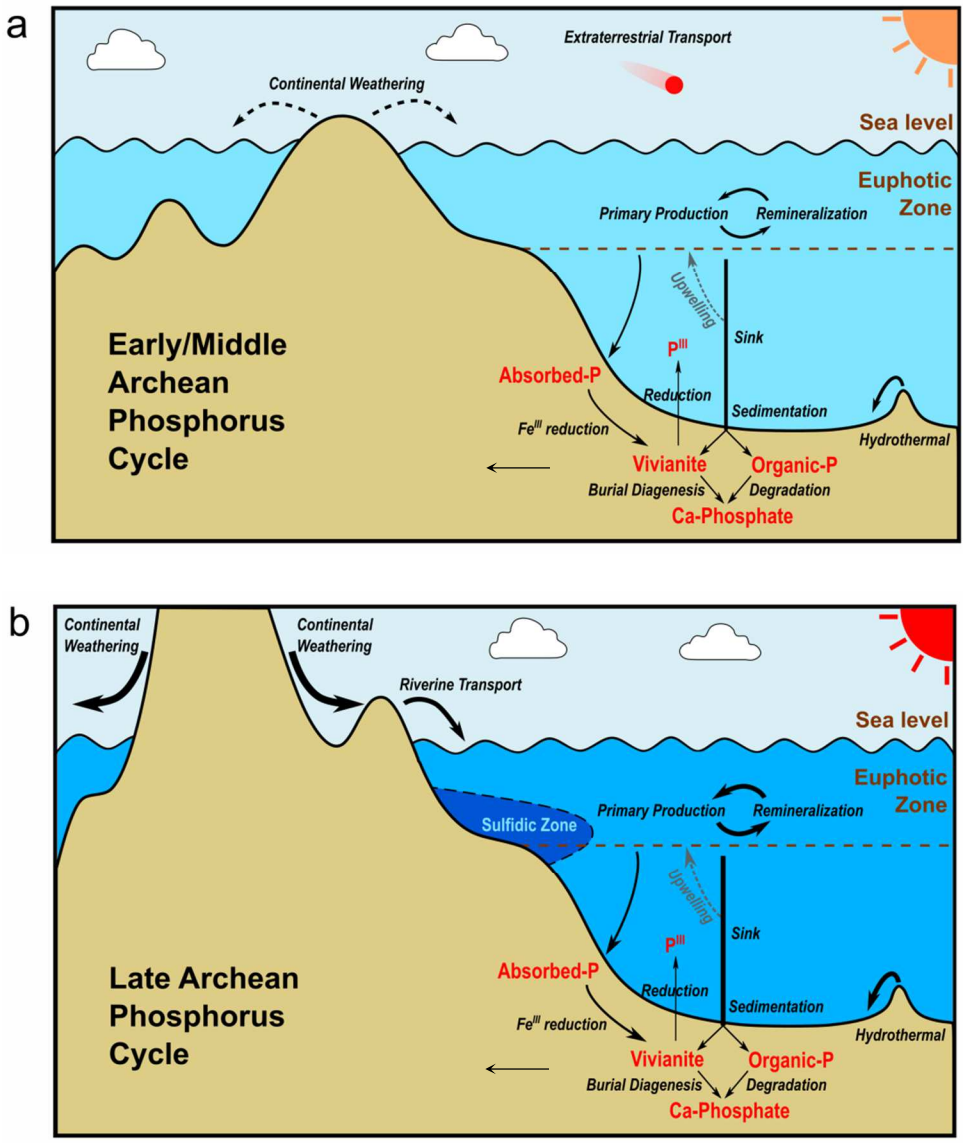

Fig. 9. Reconstructed phosphorus cycle in the early/middle Archean (a) and late Archean (b) worlds. The intensity of seawater color indicates relative levels of P, i.e. thin blue, medium blue, and dark blue represent low, medium, and high P concentration, respectively. Arrow weights indicate the relative flux of constituent processes within the P cycle (smaller flux by thin lines and greater flux by thick lines). Dashed lines or regions indicate processes presumed to be weak or only expressed locally.

772 Table 1. Fluxes of bioavailable or biological P in the modern and early Earth (in 10^{10}
773 moles/yr).

P fluxes*	**Pre-industrial Earth**	**Early Archean Earth**	**Late Archean Earth**
Continental input[a]	10-15 [a] (+)	~0 (+)	4-34 [b] (+)
Recycling of organic P	~3710 [c] (+)	< 0.04 (+)	14-120 (+)[d]
Seafloor weathering[e]	10-36 [f] (-)	(-)	>4 (-)
Extraterrestrial	(+)	< 0.01 [g] (+)	< 0.01 (+)
Total P for net primary production[h]	3720 [c]	< 0.05	18-154

774 *Plus sign (+) represents source and minus sign (-) sink.

775 [a]Reactive P = Dissolved inorganic P + Dissolved organic P + Particulate organic P + Iron-
776 bound particulate P + Reactive aeolian P (Compton et al., 2010); [b]Hao et al. (2020);
777 [c]Schlesiner & Bernhardt (2013); [d]Optimisitic estimate calculated with equation (6-8)
778 assuming $R_{recycling}$ = 0.78 (Sec. 3.3 in main text); [e]Seafloor weathering (-) = hydrothermal
779 deposition (-) + seafloor sedimentation (-) = continental input (+) + extraterrestrial input (+);
780 [f]Paytan & McLaughlin (2007); [g]Tsukamoto et al. (2018); [h]NPP(P) = continental input +
781 recycling of organic P + extraterrestrial

782

Research Data Thermodynamic properties of chemical reactions are provided in supplementary file. The continental weathering and seawater chemistry models are calculated using the codes shared online by Krissansen-Totton (https://github.com/joshuakt/early-earth-carbon-cycle) with additional modifications on continental emergence (see main text).

788 **References:**

789 Al-Borno A. and Tomson M. B. (1994) The temperature dependence of the solubility product
790 constant of vivianite. *Geochim. Cosmochim. Acta* **58**, 5373–5378.

791 Alt, J.C. and Honnorez, J. (1984) Alteration of the upper oceanic crust, DSDP site 417:
792 mineralogy and chemistry. *Contrib. Mineral. Petr.* 87, 149-169.

793 Anbar A. D., Duan Y., Lyons T. W., Arnold G. L., Kendall B., Creaser R. A., Kaufman A. J.,
794 Gordon G. W., Scott C., Garvin J. and Buick R. (2007) A whiff of oxygen before the
795 great oxidation event? *Science (80-.).* **317**, 1903–1906.

796 Anderson A. T. and Greenland L. P. (1969) Phosphorus fractionation diagram as a
797 quantitative indicator of crystallization differentiation of basaltic liquids. *Geochim.*
798 *Cosmochim. Acta* **33**, 493–505.

799 Baturin G. (2003) Phosphorus cycle in the ocean. *Lithol. Miner. Resour.* **38**, 101–119.

800 Bindeman I. N., Zakharov D. O., Palandri J., Greber N. D., Dauphas N., Retallack G. J.,
801 Hofmann A., Lackey J. S. and Bekker A. (2018) Rapid emergence of subaerial
802 landmasses and onset of a modern hydrologic cycle 2.5 billion years ago. *Nature* **557**,
803 545–548.

804 Bjerrum C. J. and Canfield D. E. (2002) Ocean productivity before about 1.9 Gyr ago limited
805 by phosphorus adsorption onto iron oxides. *Nature* **417**, 159–162.

806 Borch T. and Fendorf S. (2007) Chapter 12 Phosphate Interactions with Iron (Hydr)oxides:
807 Mineralization Pathways and Phosphorus Retention upon Bioreduction. In
808 *Developments in Earth and Environmental Sciences* (eds. M. O. Barnett and D. B. Kent).
809 Elsevier. pp. 321–348.

810 Brantley S. L. and Olsen A. A. (2014) Reaction Kinetics of Primary Rock-Forming Minerals
811 under Ambient Conditions. In *Treatise on Geochemistry: Second Edition* (eds. H. D.
812 Holland and K. K. Turekian). Elsevier, Oxford. pp. 69–113.

Brunet F. and Chazot G. (2001) Partitioning of phosphorus between olivine, clinopyroxene and silicate glass in an spinel lherzolite xenolith from Yemen. *Chem. Geol.* **176**, 51–72.

Byrne R. H. and Kim K. H. (1993) Rare earth precipitation and coprecipitation behavior: The limiting role of PO43- on dissolved rare earth concentrations in seawater. *Geochim. Cosmochim. Acta* **57**, 519–526.

Canfield D. E., Rosing M. T. and Bjerrum C. (2006) Early anaerobic metabolisms. *Philos. Trans. R. Soc. B Biol. Sci.* **361**, 1819–1834.

Cardona T., Sánchez-Baracaldo P., Rutherford A. W. and Larkum A. W. (2019) Early Archean origin of Photosystem II. *Geobiology* **17**, 127–150.

Chameides W. L. and Walker J. C. G. (1981) Rates of fixation by lightning of carbon and nitrogen in possible primitive atmospheres. *Orig. Life* **11**, 291–302.

Clark L. L., Ingall E. D. and Benner R. (1998) Marine phosphorus is selectively remineralized. *Nature* **393**, 426.

Compton J., Mallinson D., Glenn C. R., Filippelli G., Follmi K., Shields G. and Zanin Y. (2010) Variations in the Global Phosphorus Cycle. *Mar. Authigenes. From Glob. to Microb.*, 21–33.

Coogan L. A., MacLeod C. J., Dick H. J. B., Edwards S. J., Kvassnes A., Natland J. H., Robinson P. T., Thompson G. and O'Hara M. J. (2001) Whole-rock geochemistry of gabbros from the Southwest Indian Ridge: Constraints on geochemical fractionations between the upper and lower oceanic crust and magma chamber processes at (very) slow-spreading ridges. *Chem. Geol.* **178**, 1–22.

Cosmidis J., Benzerara K., Morin G., Busigny V., Lebeau O., Jézéquel D., Noël V., Dublet G. and Othmane G. (2014) Biomineralization of iron-phosphates in the water column of Lake Pavin (Massif Central, France). *Geochim. Cosmochim. Acta* **126**, 78–96.

Crowe S. A., Katsev S., Leslie K., Sturm A., Magen C., Nomosatryo S., Pack M. A., Kessler

J. D., Reeburgh W. S., Roberts J. A., González L., Douglas Haffner G., Mucci A., Sundby B. and Fowle D. A. (2011) The methane cycle in ferruginous Lake Matano. *Geobiology* **9**, 61–78.

de Kanel J. and Morse J. W. (1978) The chemistry of orthophosphate uptake from seawater on to calcite and aragonite. *Geochim. Cosmochim. Acta* **42**, 1335–1340.

Derry L. A. (2015) Causes and consequences of mid-Proterozoic anoxia. *Geophys. Res. Lett.* **42**, 8538–8546.

Eanes E. D. and Meyer J. L. (1977) The maturation of crystalline calcium phosphates in aqueous suspensions at physiologic pH. *Calcif. Tissue Res.* **23**, 259–269.

Falkowski P. G. (1997) Evolution of the nitrogen cycle and its influence on the biological sequestration of CO2 in the ocean. *Nature* **387**, 272–275.

Field C. B., Behrenfeld M. J., Randerson J. T. and Falkowski P. (1998) Primary production of the biosphere: Integrating terrestrial and oceanic components. *Science (80-.).* **281**, 237–240.

Fischer W. W., Hemp J. and Johnson J. E. (2016) Evolution of Oxygenic Photosynthesis. *Annu. Rev. Earth Planet. Sci.* **44**, 647–683.

Flament N., Coltice N. and Rey P. F. (2013) The evolution of the87Sr/86Sr of marine carbonates does not constrain continental growth. *Precambrian Res.* **229**, 177–188.

Fourqurean J. W., Zieman J. C. and Powell G. V. N. (1992) Phosphorus limitation of primary production in Florida Bay: Evidence from C:N:P ratios of the dominant seagrass Thalassia testudinum. *Limnol. Oceanogr.* **37**, 162–171.

Francko D. A. and Heath R. T. (1979) Functionally distinct classes of complex phosphorus compounds in lake water. *Limnol. Oceanogr.* **24**, 463–473.

Freeman J. S. and Rowell D. L. (1981) The adsorption and precipitation of phosphate onto calcite. *J. Soil Sci.* **32**, 75–84.

863 Friend C. R. L., Nutman A. P., Bennett V. C. and Norman M. D. (2008) Seawater-like trace
864 element signatures (REE + Y) of Eoarchaean chemical sedimentary rocks from southern
865 West Greenland, and their corruption during high-grade metamorphism. *Contrib. to*
866 *Mineral. Petrol.* **155**, 229–246.
867 Geider R. J. and La Roche J. (2002) Redfield revisited: Variability of C:N:P in marine
868 microalgae and its biochemical basis. *Eur. J. Phycol.* **37**, 1–17.
869 Green T. H. and Watson E. B. (1982) Crystallization of apatite in natural magmas under high
870 pressure, hydrous conditions, with particular reference to "Orogenic" rock series.
871 *Contrib. to Mineral. Petrol.* **79**, 96–105.
872 Guidry M. W. and Mackenzie F. T. (2003) Experimental study of igneous and sedimentary
873 apatite dissolution. *Geochim. Cosmochim. Acta* **67**, 2949–2963.
874 Gunnars A., Blomqvist S. and Martinsson C. (2004) Inorganic formation of apatite in
875 brackish seawater from the Baltic Sea: An experimental approach. *Mar. Chem.* **91**, 15-
876 26.
877 Halevy I. and Bachan A. (2017) The geologic history of seawater pH. *Science (80-.).* **355**,
878 1069–1071.
879 Hamilton T. L. (2019) The trouble with oxygen: The ecophysiology of extant phototrophs
880 and implications for the evolution of oxygenic photosynthesis. *Free Radic. Biol. Med.* **in**
881 **press**. Doi: 10.1016/j.freeradbiomed.2019.05.003
882 Hansen B. C. H. and Poulsen I. F. (1999) Interaction of synthetic sulphate green rust with
883 phosphate and the crystallization of vivianite. *Clays Clay Miner.* **47**, 312–318.
884 Hao J., Sverjensky D. A. and Hazen R. M. (2017) Mobility of nutrients and trace metals
885 during weathering in the late Archean. *Earth Planet. Sci. Lett.* **471**, 148–159.
886 Hao J., Sverjensky D. A. and Hazen R. M. (2019) Redox states of Archean surficial
887 environments: The importance of H2,g instead of O2,g for weathering reactions. *Chem.*

888 *Geol.* **521**, 49–58.
889 Hao J., Knoll A. H., Huang F., Hazen R. M. and Daniel I. (2020) Cycling Phosphorus on the
890 Archean Earth: Part I. Continental weathering and riverine transport of phosphorus.
891 *Geochim. Cosmochim. Acta* **273**, 70–84.
892 Hartnett H. E., Keil R. G., Hedges J. I. and Devol A. H. (1998) Influence of oxygen exposure
893 time on organic carbon preservation in continental margin sediments. *Nature* **391**, 572–
894 574.
895 Hawkesworth C. J., Cawood P. A., Dhuime B. and Kemp T. I. S. (2017) Earth's Continental
896 Lithosphere Through Time. *Annu. Rev. Earth Planet. Sci.* **45**, 169–198.
897 Hedges J. I., Hu F. S., Devol A. H., Hartnett H. E., Tsamakis E. and Keil R. G. (1999)
898 Sedimentary organic matter preservation: A test for selective degradation under oxic
899 conditions. *Am. J. Sci.* **299**, 529–555.
900 Hedges J. I. and Keil R. G. (1995) Sedimentary organic matter preservation: an assessment
901 and speculative synthesis. *Mar. Chem.* **49**, 81–115.
902 Herschy B., Chang S. J., Blake R., Lepland A., Abbott-Lyon H., Sampson J., Atlas Z., Kee T.
903 P. and Pasek M. A. (2018) Archean phosphorus liberation induced by iron redox
904 geochemistry. *Nat. Commun.* **9**.
905 Isson T. T. and Planavsky N. J. (2018) Reverse weathering as a long-term stabilizer of marine
906 pH and planetary climate. *Nature* **560**, 471–475.
907 Jiang C. Z. and Tosca N. J. (2019) Fe(II)-carbonate precipitation kinetics and the chemistry
908 of anoxic ferruginous seawater. *Earth Planet. Sci. Lett.* **506**, 231–242.
909 Jilbert T. and Slomp C. P. (2013) Iron and manganese shuttles control the formation of
910 authigenic phosphorus minerals in the euxinic basins of the Baltic Sea. *Geochim.*
911 *Cosmochim. Acta* **107**, 155–169.
912 Johnson B. R., Tostevin R., Gopon P., Wells J., Robinson S. A. and Tosca N. J. (2020)

913 Phosphorus burial in ferruginous SiO2-rich Mesoproterozoic sediments. *Geology* **48**,
914 92–96.
915 Johnson J. E., Muhling J. R., Cosmidis J., Rasmussen B. and Templeton A. S. (2018) Low-
916 Fe(III) Greenalite Was a Primary Mineral From Neoarchean Oceans. *Geophys. Res. Lett.*
917 **45**, 3182–3192.
918 Johnson J. W., Oelkers E. H. and Helgeson H. C. (1992) SUPCRT92: A software package for
919 calculating the standard molal thermodynamic properties of minerals, gases, aqueous
920 species, and reactions from 1 to 5000 bar and 0 to 1000°C. *Comput. Geosci.* **18**, 899–
921 947.
922 Jones C., Nomosatryo S., Crowe S. A., Bjerrum C. J. and Canfield D. E. (2015) Iron oxides,
923 divalent cations, silica, and the early earth phosphorus crisis. *Geology* **43**, 135–138.
924 Kakegawa T. (2003) Establishment of the phosphorous cycle in early Archean oceans.
925 *Geochim. Cosmochim. Acta Suppl.* **67**, 194.
926 Katsev S. and Crowe S. A. (2015) Organic carbon burial efficiencies in sediments: The
927 power law of mineralization revisited. *Geology* **43**, 607–610.
928 Kaufman A. J., Johnston D. T., Farquhar J., Masterson A. L., Lyons T. W., Bates S., Anbar A.
929 D., Arnold G. L., Garvin J. and Buick R. (2007) Late archean biospheric oxygenation
930 and atmospheric evolution. *Science (80-.).* **317**, 1900–1903.
931 Kharecha P., Kasting J. and Siefert J. (2005) A coupled atmosphere-ecosystem model of the
932 early Archean earth. *Geobiology* **3**, 53–76.
933 Kipp M. A. (2019) Causes and consequences of high burial efficiency in the Archean ocean.
934 In *2nd Geobiology Society Conference*
935 Kipp M. A. and Stüeken E. E. (2017) Biomass recycling and Earth's early phosphorus cycle.
936 *Sci. Adv.* **3**.
937 Konhauser K. O., Lalonde S. V, Amskold L. and Holland H. D. (2007) Was there really an

938 Archean phosphate crisis? *Science (80-.).* **315**, 1234.
939 Kopp R. E., Kirschvink J. L., Hilburn I. A. and Nash C. Z. (2005) The Paleoproterozoic
940 snowball Earth: A climate disaster triggered by the evolution of oxygenic photosynthesis.
941 *Proc. Natl. Acad. Sci.* **102**, 11131–11136.
942 Korenaga J., Planavsky N. J. and Evans D. A. D. (2017) Global water cycle and the
943 coevolution of the Earth's interior and surface environment. *Philos. Trans. R. Soc. A*
944 *Math. Phys. Eng. Sci.* **375**.
945 Kraal P., Dijkstra N., Behrends T. and Slomp C. P. (2017) Phosphorus burial in sediments of
946 the sulfidic deep Black Sea: Key roles for adsorption by calcium carbonate and apatite
947 authigenesis. *Geochim. Cosmochim. Acta* **204**, 140–158.
948 Krajewski K. P., Cappellen P. van, Trichet J., Kuhn O., LuCAs J., Martín-Algarra A., Prevot
949 L., Tewari V. C., Gaspar L. and Knight R. I. (1994) Biological processes and apatite
950 formation in sedimentary environments. *Eclogae Geol. Helv.* **87**, 701–746.
951 Krissansen-Totton J., Arney G. N. and Catling D. C. (2018) Constraining the climate and
952 ocean pH of the early Earth with a geological carbon cycle model. *Proc. Natl. Acad. Sci.*,
953 201721296.
954 Kuntz L. B., Laakso T. A., Schrag D. P. and Crowe S. A. (2015) Modeling the carbon cycle
955 in Lake Matano. *Geobiology* **13**, 454–461.
956 Laakso T. A. and Schrag D. P. (2018) Limitations on Limitation. *Global Biogeochem. Cycles*
957 **32**, 486–496.
958 Lenstra W. K., Egger M., van Helmond N. A. G. M., Kritzberg E., Conley D. J. and Slomp C.
959 P. (2018) Large variations in iron input to an oligotrophic Baltic Sea estuary: impact on
960 sedimentary phosphorus burial. *Biogeosciences Discuss.* **15**, 6979–6996.
961 Lepland A., Arrhenius G. and Cornell D. (2002) Apatite in early Archean Isua supracrustal
962 rocks, southern West Greenland: Its origin, association with graphite and potential as a

963 biomarker. *Precambrian Res.* **118**, 221–241.
964 Liu J., Cheng X., Qi X., Li N., Tian J., Qiu B., Xu K. and Qu D. (2018) Recovery of
965 phosphate from aqueous solutions via vivianite crystallization: Thermodynamics and
966 influence of pH. *Chem. Eng. J.* **349**, 37–46.
967 Logan G. A., Hayes J. M., Hieshima G. B. and Summons R. E. (1995) Terminal Proterozoic
968 reorganization of biogeochemical cycles. *Nature* **376**, 53–56.
969 Lyons T. W. and Gill B. C. (2010) Ancient Sulfur Cycling and Oxygenation of the Early
970 Biosphere. *Elements* **6**, 93–99.
971 Madsen H. E. L. (2019) Influence of calcium and aluminum on crystallization of vivianite,
972 Fe3(PO4)2·8H2O. *J. Cryst. Growth* **526**, 125242.
973 Madsen H. E. L. and Hansen H. C. B. (2014) Kinetics of crystal growth of vivianite,
974 Fe3(PO4)2·8H2O, from solution at 25, 35 and 45 °C. *J. Cryst. Growth* **401**, 82–86.
975 Marty B., Avice G., Bekaert D. V. and Broadley M. W. (2018) Salinity of the Archaean
976 oceans from analysis of fluid inclusions in quartz. *Comptes Rendus - Geosci.* **350**, 154–
977 163.
978 Meurer W. P. and Natland J. H. (2001) Apatite compositions from oceanic cumulates with
979 implications for the evolution of mid-ocean ridge magmatic systems. *J. Volcanol.*
980 *Geotherm. Res.* **110**, 281–298.
981 Millero F., Huang F., Zhu X., Liu X. and Zhang J. Z. (2001) Adsorption and desorption of
982 phosphate on calcite and aragonite in seawater. *Aquat. Geochemistry* **7**, 33–56.
983 Murakami A., Sawaki Y., Ueda H., Orihashi Y., Machida S., and Komiya T. (2019) Behavior
984 of phosphorus during hydrothermal alteration of basalt under CO2-rich condition. In
985 *Japan Geoscience Union Meeting 2019*
986 Nancollas G. H. (1984) The Nucleation and Growth of Phosphate Minerals. In *Phosphate*
987 *Minerals* (eds. J. O. Nriagu and P. B. Moore). Springer Berlin Heidelberg, Berlin,

Heidelberg. pp. 137–154.

Olson S. L., Jansen M. and Abbot D. S. (2019) Oceanographic Constraints on Exoplanet Life. *arXiv Prepr. arXiv1909.02928*.

Oxmann J. F. and Schwendenmann L. (2015) Authigenic apatite and octacalcium phosphate formation due to adsorption–precipitation switching across estuarine salinity gradients. *Biogeosciences* **12**, 723–738.

Paytan A. and McLaughlin K. (2007) The oceanic phosphorus cycle. *Chem. Rev.* **107**, 563–576.

Planavsky N. J., Rouxel O. J., Bekker A., Lalonde S. V, Konhauser K. O., Reinhard C. T. and Lyons T. W. (2010) The evolution of the marine phosphate reservoir. *Nature* **467**, 1088–1090.

Rasmussen B. (2000) The impact of early-diagenetic aluminophosphate precipitation on the oceanic phosphorus budget. *Mar. Authigenes. From Glob. to Microb.*, 89–101.

Rasmussen B., Muhling J. R., Suvorova A. and Krapež B. (2016) Dust to dust: Evidence for the formation of "primary" hematite dust in banded iron formations via oxidation of iron silicate nanoparticles. *Precambrian Res.* **284**, 49–63.

Reinhard C. T., Planavsky N. J., Gill B. C., Ozaki K., Robbins L. J., Lyons T. W., Fischer W. W., Wang C., Cole D. B. and Konhauser K. O. (2017) Evolution of the global phosphorus cycle. *Nature* **541**, 386–389.

Reinhard C. T., Raiswell R., Scott C., Anbar A. D. and Lyons T. W. (2009) A Late Archean Sulfidic Sea Stimulated by Early Oxidative Weathering of the Continents. *Science (80-.).* **326**, 713–716.

Rothe M., Kleeberg A., Grüneberg B., Friese K., Pérez-Mayo M. and Hupfer M. (2015) Sedimentary sulphur:iron ratio indicates vivianite occurrence: A study from two contrasting freshwater systems. *PLoS One* **10**.

1013 Rothe M., Kleeberg A. and Hupfer M. (2016) The occurrence, identification and
1014 environmental relevance of vivianite in waterlogged soils and aquatic sediments. *Earth-*
1015 *Science Rev.* **158**, 51–64.
1016 Rubinstein N., Fazio A. M., Scasso R. A. and Carey S. (2013) Association of phosphate with
1017 rhyolite glass in marine Neogene tuffs from Patagonia, Argentina. *Sedimentology* **60**,
1018 1007–1016.
1019 Ruttenberg K. C. (2014) The Global Phosphorus Cycle. In *Treatise on Geochemistry: Second*
1020 *Edition* (eds. H. D. Holland and K. K. Turekian). Elsevier, Oxford. pp. 499–558.
1021 Sánchez-Román M., Puente-Sánchez F., Parro V. and Amils R. (2015) Nucleation of Fe-rich
1022 phosphates and carbonates on microbial cells and exopolymeric substances. *Front.*
1023 *Microbiol.* **6**.
1024 Schieber J., Sur S. and Banerjee S. (2007) Benthic microbial mats in black shale units from
1025 the Vindhyan Supergroup, Middle Proterozoic of India: the challenges of recognizing
1026 the genuine article. *Atlas Microb. mat Featur. Preserv. within clastic rock Rec.*
1027 *Amsterdam, Elsevier*, 189–197.
1028 Schlesinger W. H. and Bernhardt E. S. (2013) *Biogeochemistry: an analysis of global*
1029 *change*., Academic press.
1030 Schneiderhan E., Zimmermann U., Gutzmer J., Mezger K. and Armstrong R. (2011)
1031 Sedimentary provenance of the neoarchean ventersdorp supergroup, Southern Africa:
1032 Shedding light on the evolution of the kaapvaal craton during the neoarchean. *J. Geol.*
1033 **119**, 575–596.
1034 Siever R. (1992) The silica cycle in the Precambrian. *Geochim. Cosmochim. Acta* **56**, 3265–
1035 3272.
1036 Sleep N. H. and Zahnle K. (2001) Carbon dioxide cycling and implications for climate on
1037 ancient Earth. *J. Geophys. Res.* **106**, 1373.

1038 Staudigel H., Furnes H., McLoughlin N., Banerjee N. R., Connell L. B. and Templeton A.
1039 (2008) 3.5 billion years of glass bioalteration: Volcanic rocks as a basis for microbial
1040 life? *Earth-Science Rev.* **89**, 156–176.
1041 Stüeken E. E., Catling D. C. and Buick R. (2012) Contributions to late Archaean sulphur
1042 cycling by life on land. *Nat. Geosci.* **5**, 722–725.
1043 Syverson D. D., Reinhard C. T., Isson T. T., Holstege C., Katchinoff J., Tutolo B. M.,
1044 Etschmann B., Brugger J. and Planavsky N. J. (2020) Anoxic weathering of mafic
1045 oceanic crust promotes atmospheric oxygenation. *arXiv Prepr. arXiv2002.07667*.
1046 Thinnappan V., Merrifield C. M., Islam F. S., Polya D. A., Wincott P. and Wogelius R. A.
1047 (2008) A combined experimental study of vivianite and As (V) reactivity in the pH
1048 range 2–11. *Appl. Geochemistry* **23**, 3187–3204.
1049 Tosca N. J., Guggenheim S. and Pufahl P. K. (2016) An authigenic origin for Precambrian
1050 greenalite: Implications for iron formation and the chemistry of ancient seawater. *Bull.*
1051 *Geol. Soc. Am.* **128**, 511–530.
1052 Tosca N. J., Jiang C. Z., Rasmussen B. and Muhling J. (2019) Products of the iron cycle on
1053 the early Earth. *Free Radic. Biol. Med.* **in press**. Doi:
1054 10.1016/j.freeradbiomed.2019.05.005
1055 Tréguer P. J. and De La Rocha C. L. (2012) The World Ocean Silica Cycle. *Ann. Rev. Mar.*
1056 *Sci.* **5**, 477–501.
1057 Tsukamoto Y., Kakegawa T., Graham U., Liu Z.-K., Ito A. and Ohmoto H. (2018) Discovery
1058 of Ni-Fe Phosphides in the 3.46 Ga-Old Apex Basalt: Implications on the Phosphate
1059 Budget of the Archean Oceans. *Goldschmidt Abstr.*
1060 Tyrrell T. (1999) The relative influences of nitrogen and phosphorus on oceanic primary
1061 production. *Nature* **400**, 525–531.
1062 Van Cappellen P. S. and Berner R. A. (1991) The formation of marine apatite: A kinetic

1063 study. Yale University.
1064 Vuillemin A., Wirth R., Kemnitz H., Schleicher A. M., Friese A., Bauer K. W., Simister R.,
1065 Nomosatryo S., Ordoñez L., Ariztegui D., Henny C., Crowe S. A., Benning L. G.,
1066 Kallmeyer J., Russell J. M., Bijaksana S., Vogel H. and Team the T. D. P. S. (2019)
1067 Formation of diagenetic siderite in modern ferruginous sediments. *Geology* **47**, 540–544.
1068 Walpersdorf E., Koch C. B., Heiberg L., O'Connell D. W., Kjaergaard C. and Hansen H. C.
1069 B. (2013) Does vivianite control phosphate solubility in anoxic meadow soils?
1070 *Geoderma* **193–194**, 189–199.
1071 Ward L. M., Kirschvink J. L. and Fischer W. W. (2016) Timescales of Oxygenation
1072 Following the Evolution of Oxygenic Photosynthesis. *Orig. Life Evol. Biosph.* **46**, 51–65.
1073 Ward L. M., Rasmussen B. and Fischer W. W. (2019) Primary Productivity Was Limited by
1074 Electron Donors Prior to the Advent of Oxygenic Photosynthesis. *J. Geophys. Res.*
1075 *Biogeosciences* **124**, 211–226.
1076 Wheat C. G., Feely R. A. and Mottl M. J. (1996) Phosphate removal by oceanic hydrothermal
1077 processes: An update of the phosphorus budget in the oceans. *Geochim. Cosmochim.*
1078 *Acta* **60**, 3593–3608.
1079 Wong M. L., Charnay B. D., Gao P., Yung Y. L. and Russell M. J. (2017) Nitrogen Oxides in
1080 Early Earth's Atmosphere as Electron Acceptors for Life's Emergence. *Astrobiology* **17**,
1081 975–983.
1082 Xiong Y. (2019) Phosphorus cycling under different redox conditions. University of Leeds .
1083 Xu N., Chen M., Zhou K., Wang Y., Yin H. and Chen Z. (2014) Retention of phosphorus on
1084 calcite and dolomite: speciation and modeling. *RSC Adv.* **4**, 35205–35214.
1085 Zegeye A., Bonneville S., Benning L. G., Sturm A., Fowle D. A., Jones C. A., Canfield D. E.,
1086 Ruby C., MacLean L. C., Nomosatryo S., Crowe S. A. and Poulton S. W. (2012) Green
1087 rust formation controls nutrient availability in a ferruginous water column. *Geology* **40**,

599–602.

Zonneveld K. A. F., Versteegh G. J. M., Kasten S., Eglinton T. I., Emeis K. C., Huguet C., Koch B. P., De Lange G. J., De Leeuw J. W., Middelburg J. J., Mollenhauer G., Prahl F. G., Rethemeyer J. and Wakeham S. G. (2010) Selective preservation of organic matter in marine environments; Processes and impact on the sedimentary record. *Biogeosciences* **7**, 483–511.